

TILDEN LECTURE*

The Properties of Hydrogen-bonded Dimers from Rotational Spectroscopy

By A. C. Legon

DEPARTMENT OF CHEMISTRY, UNIVERSITY COLLEGE LONDON,
20 GORDON STREET, LONDON WC1H 0AJ

1 Introduction

The hydrogen bond has a sufficiently familiar rôle in nature that it would be superfluous to rehearse in detail here evidence for either its ubiquity or its importance. To refer to just one simple consequence of the existence of the hydrogen bond: water would be a gas at room temperature were it not for this interaction and life on earth would not be possible in its present form. Investigations that lead to an understanding of the nature of the hydrogen bond are consequently worthwhile pursuits that can be readily justified.

In the context of the present article, to understand the hydrogen bond means to know experimentally the various properties of the molecules containing the bond and then to be able to predict these by means of a model. In turn, this means identifying the properties of most interest. We shall here restrict attention to the interaction of *two* molecules B and HX. When they are bound together (through *e.g.* a hydrogen bond) we shall refer to the molecule B...HX as a *dimer* (when B and HX are identical molecules, as in HCN...HCN, we can formally describe the associated species as a *homodimer*, otherwise the composite molecule is a *heterodimer*). The primary properties of a hydrogen-bonded dimer are, for example, the relative position and orientation of the component subunits in space (the radial and angular geometry), the strength with which the two components are held together (the energy required to dissociate the dimer into the subunits or the restoring force per unit infinitesimal displacement along the dissociation coordinate), and the changes (both geometrical and electrical) occurring within the subunits when the bond is formed.

It is well known that the hydrogen bond is usually a relatively weak interaction (typically, the dissociation energy D_0 and the restoring force constant k_σ lie in the ranges 10–50 kJ mol⁻¹ and 5–20 N m⁻¹, respectively). Clearly, for purposes of comparing experiment and theory, it is desirable to determine what might be called the *intrinsic* properties of the hydrogen bond *i.e.* those pertaining to the isolated dimer, free from the effects of nearby molecules such as are present in solution, in molecular crystals or even in an inert matrix in matrix isolation experiments. A useful way of determining the *intrinsic* properties of dimers

* This is an extended version of the Tilden Lecture presented at a meeting of the Faraday Division of the Royal Society of Chemistry held at the Scientific Societies' Lecture Theatre, London, on 26 April 1990.

$B \cdots HX$ is from their rotational spectra since such spectra are recorded at low pressure in the gas phase and refer to the effectively isolated molecule.

The properties of $B \cdots HX$ described here have been determined by rotational spectroscopy with the aid mainly of the techniques of Stark-modulation microwave spectroscopy and pulsed-nozzle Fourier-transform microwave spectroscopy. These techniques and their advantages are described in outline in Section 2. A summary of various properties of $B \cdots HX$ available from rotational spectroscopy is then given in Section 3 by reference to the prototype dimer $HCN \cdots HF$. Section 4, the main part of this review, consists of some generalizations that it has been possible to make about hydrogen-bonded dimers $B \cdots HX$ by investigating carefully chosen series along which B or HX is allowed to vary.

2 Methods of Observing the Rotational Spectra of Hydrogen-bonded Dimers

$B \cdots HX$

In general, the rotational spectra of hydrogen-bonded (and other weakly bound) dimers have been observed by using three techniques: Stark-modulation microwave spectroscopy, molecular beam electric resonance spectroscopy (MBERS), and pulsed-nozzle, Fourier-transform microwave spectroscopy. Each has been described in detail elsewhere¹⁻⁵ and it is sufficient to give here only brief outlines which highlight the advantages and disadvantages.

Stark-modulation microwave spectroscopy has been widely used to observe rotational spectra for many years. Monochromatic microwave radiation passes through a gas contained at thermal and hydrostatic equilibrium in a long waveguide absorption cell. The gas is subjected (*via* an alternating, zero-based square wave potential applied to a central electrode) to an electric field which is switched on and off with a frequency of, typically, between 5 and 100 kHz. During the 'on' half-cycle the uniform static electric field splits rotational energy levels (and transitions) into several components through the Stark effect. If the applied electric field strength is sufficient, a rotational transition that is resonant with the microwave radiation during the 'off' half-cycle is shifted out of resonance during the other half-cycle. The microwave radiation emerging from the gas is thereby intensity modulated by molecular absorption at a frequency equal to that of the square wave and can be detected with high sensitivity at this frequency by standard methods.

When the rotational spectra of dimers $B \cdots HX$ are detected by the Stark modulation microwave technique³ the waveguide absorption cell containing a mixture of B and HX is usually cooled to ≈ 200 K. The cooling is required to enhance the number of dimers present because rotational spectroscopy is

¹ T. R. Dyke, *Top. Curr. Chem.*, 1984, **120**, 85.

² T. R. Dyke and J. S. Muentner in 'International Review of Science: Physical Chemistry Series Two', ed. A. D. Buckingham, Butterworths, London, 1975, Vol. 2.

³ A. C. Legon, D. J. Millen, and S. C. Rogers, *Proc. R. Soc. London, Ser. A*, 1980, **370**, 213.

⁴ T. J. Balle and W. H. Flygare, *Rev. Sci. Instrum.*, 1981, **52**, 33.

⁵ A. C. Legon, *Annu. Rev. Phys. Chem.*, 1983, **34**, 275.

conducted at low pressure and the equilibrium constant for the reaction



is small at normal temperatures. Obviously, there is an optimum value for the temperature. This is determined by the competition between the decreasing vapour pressure of the solid $B \cdots HX$ and the increasing equilibrium constant as T decreases, since eventually the loss of dimer by condensation is greater than the gain resulting from increase of the equilibrium constant for reaction 1. For weakly bound dimers, condensation usually wins before the number of dimers reaches a value that is observable within the sensitivity limit of the spectrometer. On the other hand, for more strongly bound dimers such as $\text{HCN} \cdots \text{HF}$,³ $\text{CH}_3\text{CN} \cdots \text{HF}$,⁶ $\text{H}_2\text{O} \cdots \text{HF}$,^{7,8} $\text{D}_2\text{O} \cdots \text{HF}$,⁹ and $\text{C}_2\text{H}_2 \cdots \text{HF}$,¹⁰ rotational transitions have an optimum intensity that is readily observable. The optimum temperature in these cases lies in the range 200 to 250 K. An example of a rotational spectrum detected in this way is given in Figure 1 which shows the $J = 5 \leftarrow 4$ transition of the linear dimer $\text{HC}^{14}\text{N} \cdots \text{HF}$. The rotational transition in the vibrational ground state is indicated. The remaining features correspond to the same rotational transition but in different vibrational states (*i.e.* vibrational satellites). At the temperature of the experiment (~ 200 K), only the low-wavenumber vibrational modes of the dimer are sufficiently populated. These correspond to the intermolecular stretching (ν_o) and bending (ν_b) modes, drawn schematically in Figure 1. Vibrational satellites provide an important route to the characterization of intermolecular modes³ (see Section 3). Another advantage of Stark-modulation microwave spectroscopy lies in the simultaneous observation of the zero-field transition (upward pointing in Figure 1) and the Stark effect (downward pointing lobes) 180° out of phase. The Stark effect is a useful aid to spectral assignment and allows the electric dipole moment of the dimer to be measured.^{3,9,11}

The condensation of dimers on cooling an equilibrium gas mixture of B and HX is a serious limitation to the study of hydrogen-bonded dimers by the Stark-modulation method. Clearly, it is desirable somehow to cool a gas while simultaneously avoiding condensation. Such a result can be achieved by the well known method of diluting the two components B and HX in argon and expanding the resulting gas mixture (usually held at room temperature and a pressure in the range 1–5 atm.) adiabatically through a small nozzle into a vacuum. The result is a jet (when no collimation is imposed) or a molecular beam (collimation) and in either case consists of molecules that are in collisionless expansion when a distance of only approx. 10 nozzle diameters has been

⁶ J. W. Bevan, A. C. Legon, D. J. Millen, and S. C. Rogers, *Proc. R. Soc. London, Ser. A*, 1980, **370**, 239.

⁷ J. W. Bevan, Z. Kisiel, A. C. Legon, D. J. Millen, and S. C. Rogers, *Proc. R. Soc. London, Ser. A*, 1980, **372**, 441.

⁸ Z. Kisiel, A. C. Legon, and D. J. Millen, *Proc. R. Soc. London, Ser. A*, 1982, **381**, 419.

⁹ A. S. Georgiou, A. C. Legon, and D. J. Millen, *Proc. R. Soc. London, Ser. A*, 1980, **373**, 511.

¹⁰ A. S. Georgiou, A. C. Legon, and D. J. Millen, *J. Mol. Struct.*, 1980, **69**, 69.

¹¹ Z. Kisiel, A. C. Legon, and D. J. Millen, *J. Chem. Phys.*, 1983, **78**, 2910.

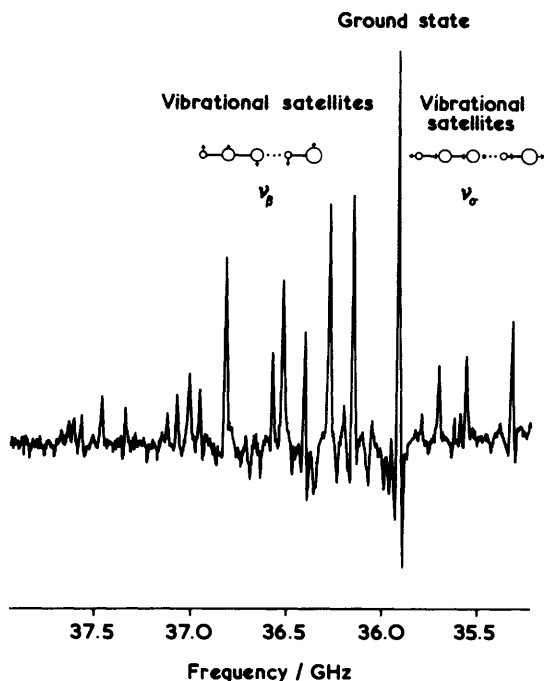


Figure 1 $J = 5 \leftarrow 4$ rotational transition in $\text{HC}^{14}\text{N}\cdots\text{HF}$ recorded with a Stark-modulation microwave spectrometer. The waveguide absorption cell contained an equilibrium mixture of HCN , HF , and $\text{HCN}\cdots\text{HF}$ at a temperature of ≈ 200 K and a pressure of ≈ 150 mTorr. The vibrational ground-state transition is indicated. Vibrational satellites associated with the hydrogen-bond stretching mode ν_s and the hydrogen-bond bending mode ν_b occur to low and high frequency, respectively, of the ground-state transition (Redrawn from ref. 33 with permission of the Royal Society of Chemistry)

traversed after emerging from the nozzle. The expanding gas is relatively rich in dimers $\text{B}\cdots\text{HX}$ and moreover during the expansion phase there is a dramatic lowering of the effective temperature of these molecules. Thus, speeds in the jet direction are all narrowly distributed about the value $\approx 5 \times 10^4$ cm s^{-1} while in transverse directions the relative speeds are close to zero. There is also considerable cooling of the internal modes of $\text{B}\cdots\text{HX}$, especially the rotational motion and the intermolecular vibrational modes. Once in collisionless expansion the dimers are in their lowest energy states and consequently in general have no mechanism, either unimolecular or bimolecular, by means of which to dissociate. They can then be probed by microwave radiation in the relatively long time period before they are destroyed by collisions with the walls of the evacuated vessel. Clearly, the long, narrow waveguides in which microwave spectroscopy is usually conducted are not suitable for containing the adiabatically expanded gas. The molecule-radiation interactions must now be brought about in vessels of larger dimensions.

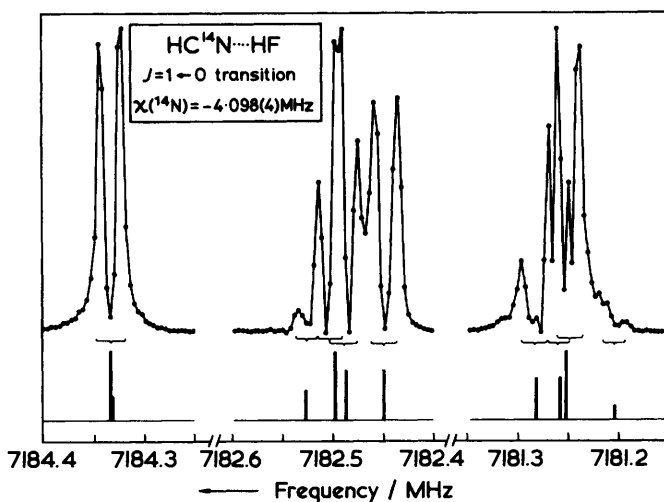


Figure 2 $J = 1 \leftarrow 0$ rotational transition of $\text{HC}^{14}\text{N}\cdots\text{HF}$ recorded with a pulsed-nozzle Fourier-transform microwave spectrometer. The gross triplet arises from ^{14}N -nuclear quadrupole coupling of the ^{14}N nuclear spin I to the rotational angular momentum J . The sub-structure on each component of the triplet arises from $\text{H}, ^{19}\text{F}$ nuclear spin-nuclear spin coupling. The stick diagram indicates the calculated pattern. Note that each observed hyperfine component is split into a doublet by the so-called Doppler doubling effect (Redrawn from ref. 12 with permission of the Royal Society)

In pulsed-nozzle, Fourier-transform microwave spectroscopy^{4,5} a pulse of microwave radiation induces a macroscopic electric rotational polarization in a pulsed jet of the expanded gas mixture. The interaction occurs in the voluminous Fabry-Pérot cavity contained in a large evacuated chamber. The subsequent decay of the polarization through spontaneous coherent emission at a rotational transition frequency of $B \cdots HX$ can be coupled out of the cavity and detected at high sensitivity in the absence of the relatively intense polarizing pulse since the latter decays very rapidly. MBERS, on the other hand, employs a collimated molecular beam.^{1,2} An inhomogeneous electric field is used to deflect molecules in a given state (and hence having a given Stark effect) into a mass spectrometer which acts as the detector. Microwave radiation crosses the beam at right angles and, when it is resonant with a particular transition, causes a change in the population of the focused state and hence in the number of molecules reaching the detector.

The advantages of the techniques based on jets or beams lie in their high sensitivity for dimers coupled with a high resolution. Collisional broadening effects, which dominate linewidths in Stark modulation microwave spectroscopy, are absent and the resolution is limited by Doppler or transit-time broadening. The sensitivity is high even for the most weakly bound dimers because (a) many dimers are formed in the expansion and (b) they persist in the collisionless expansion phase. As an example of the combined high sensitivity and high

resolution, Figure 2 shows the $J = 1 \leftarrow 0$ ground state transition of $\text{HC}^{14}\text{N} \cdots \text{HF}$.^{12 13} Individual linewidths are as low as only 10 kHz and consequently much hyperfine structure is revealed (see Section 3) A recently exploited¹⁴ advantage of pulsed-nozzle FT microwave spectroscopy follows from the fact that molecules emerging from the nozzle are in collisionless expansion after travelling only approximately 10 nozzle diameters (*e.g.* 3–7 mm) at speeds of $\sim 5 \times 10^4 \text{ cm s}^{-1}$, that is after *ca.* 10 microseconds. If two components that rapidly react with each other under normal conditions in the gas phase are kept separate and allowed to mix only at the point where they expand into the vacuum chamber, the initial, transient molecule resulting from their interaction becomes frozen after only *ca.* 10 microseconds. The transient molecule, once in collisionless expansion, has no mechanism by which to undergo further progress along the reaction coordinate to give products because of the low effective temperature. In this way, the hydrogen-bonded dimer formed between oxirane and hydrogen chloride has been isolated and characterized by means of its rotational spectrum.¹⁴ At normal temperatures and pressures, gaseous oxirane and hydrogen chloride react almost instantaneously to give the product of the ring opening reaction, 2-chloroethanol.

The disadvantage of jet/beam techniques is a concomitant of the very low effective temperature. Even the low-energy intermolecular modes of $\text{B} \cdots \text{HX}$ are not usually populated and hence vibrational satellites are not usually observed. Additionally, when argon is used as the carrier gas, only the lowest energy isomer of a given dimer is generally observed. Recently, however, work using different carrier gas mixtures has shown that it is possible to raise the effective temperature of the expanded gas and observe higher energy isomers. For example, Gutowsky and co-workers¹⁵ have published the results of elegant experiments in which the rotational spectrum of the linear, higher energy isomer

$\text{OCO} \cdots \text{HCN}$ can be observed in addition to the T-shaped form $\begin{array}{c} \text{O} \\ | \\ \text{C} \cdots \text{NCH} \\ | \\ \text{O} \end{array}$ by using Ne/He carrier gas mixtures.

3 The Properties of Dimers $\text{B} \cdots \text{HX}$ Available from Rotational Spectroscopy

The linear, hydrogen-bonded dimer $\text{HCN} \cdots \text{HF}$ has been investigated^{3 12 13} in considerable detail by two of the three techniques discussed in Section 2 and therefore provides a convenient vehicle for illustrating the wide range of properties of species $\text{B} \cdots \text{HX}$ that are available from rotational spectroscopy. The $J = 5 \leftarrow 4$ rotational transition of $\text{HCN} \cdots \text{HF}$ as observed by Stark-modulation microwave spectroscopy is shown in Figure 1. The strongest feature is the vibrational ground state transition while the remainder consists of vibrational satellites. When a single transition is examined under the higher resolution available through pulsed-nozzle, FT microwave spectroscopy, two

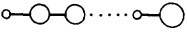
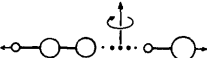
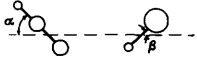
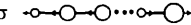
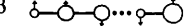
¹² A. C. Legon, D. J. Millen, and L. C. Willoughby, *Proc. R. Soc. London, Ser. A*, 1985, **401**, 327.

¹³ A. C. Legon and D. J. Millen, *Chem. Rev.*, 1986, **86**, 635.

¹⁴ A. C. Legon and C. A. Rego, *Angew. Chem., Int. Ed. Engl.*, 1990, **29**, 72.

¹⁵ T. D. Klots, R. S. Ruoff, and H. S. Gutowsky, *J. Chem. Phys.*, 1989, **90**, 4216.

Table 1 Spectroscopic quantities of B...HX, the dimer properties available from them, and their values for HCN...HF

Spectroscopic quantity/effect	Dimer Property	 H C N H F
A. Nature of rotational spectrum, rotational constants B_0 (isotopomers)	Symmetry, radial/angular geometry	collinear nuclei, $r(\text{N}\cdots\text{F}) = 2.8047(3) \text{ \AA}$
B. Centrifugal distortion constant, D_J	 Intermolecular force constant, k_σ frequency, $\tilde{\nu}_\sigma$	$k_\sigma = 18.26(5) \text{ N m}^{-1}$ $\tilde{\nu}_\sigma = 163(1) \text{ cm}^{-1}$
Absolute intensity of rot. transitions of B, HX, and B...HX in equilibrium mixture	Dissociation energy for B...HX = B + HX	$D_0 = 18.9(11) \text{ kJ mol}^{-1}$ $D_e = 26.1(16) \text{ kJ mol}^{-1}$
C. Nuclear hyperfine coupling		
^{14}N -nuclear quadrupole splitting	HCN subunit oscillation	$\cos^{-1}\langle\cos^2\alpha\rangle^{\frac{1}{2}} = 10.4^\circ$
H,F spin-spin coupling; D-nuclear quadrupole coupling	HF subunit oscillation, HF bond lengthening	$\cos^{-1}\langle\cos^2\beta\rangle^{\frac{1}{2}} = 16.1^\circ$ $\delta r = 0.011 \text{ \AA}$
D. Stark effect in rotational transitions	Electric dipole moment enhancement $\mu = \mu_B\langle\cos\alpha\rangle + \mu_{\text{HX}}\langle\cos\beta\rangle + \Delta\mu$	$\Delta\mu = 0.897(10) \text{ D}$
E. Vibrational satellites	Intermolecular modes σ  β 	
Relative intensities	Vib. separations	$\tilde{\nu}_\sigma = 1 \longleftarrow 0 \quad 197(15) \text{ cm}^{-1}$ $\tilde{\nu}_\beta = 1 \longleftarrow 0 \quad 91(20) \text{ cm}^{-1}$
l -Doubling	ν_β bending wavenumber	$\tilde{\nu}_\beta = 1 \longleftarrow 0 \quad 72(4) \text{ cm}^{-1}$
Fermi resonance	Vib. separations, cubic force constants	$\tilde{\nu}_\sigma - 2\tilde{\nu}_\beta = 16 \text{ cm}^{-1}$ $k_{\sigma\beta\beta} = 7.4 \text{ cm}^{-1}$

types of nuclear hyperfine structure are revealed, as shown for the $J = 1 \longleftarrow 0$ transition of $\text{HC}^{14}\text{N}\cdots\text{HF}$ in Figure 2. Much information about $\text{HCN}\cdots\text{HF}$ is contained in these spectra. Table 1 gives a summary of the observable spectroscopic quantities/effects (column 1), the dimer properties available from

the spectroscopic observables (column 2), and values of the dimer properties for the particular case of HCN...HF.

A. Dimer Symmetry, Radial and Angular Geometry.—The nature of the rotational spectrum can often give information about the symmetry of the dimer B...HX. For example, HCN...HF is shown in this way to be a linear species at equilibrium.³ If the intermolecular interaction is sufficiently weak, it can be assumed that the monomer geometries are sensibly unchanged on dimer formation. Under this assumption and given that the dimer is linear at equilibrium with nuclei in the order shown, the rotational constant B_0 can be used to determine the intermolecular separation as characterized by the distance $r(\text{N}\cdots\text{F})$.¹² In fact, isotopic substitution at each nucleus in turn establishes unambiguously the order HCN...HF of the nuclei.^{3,12}

For HCN...HF the angular geometry (linear) is established from the symmetry inferred from the nature of the rotational spectrum. When B...HX is an asymmetric rotor, the angular geometry of the dimer can be determined, again with unchanged monomer geometries assumed, by fitting the rotational constants A_0 , B_0 , and C_0 .

B. Strength of the Hydrogen Bond.—This can be measured in two different ways. First, the quadratic force constant k_σ associated with the hydrogen-bond stretching mode ν_σ gives a measure of the restoring force per unit infinitesimal extension of the hydrogen bond. This is available from the centrifugal distortion constant D_J by using an expression due to Millen.¹⁶ If the monomers are taken as rigid, D_J , which allows for the fact that the dimer geometry depends on rotational state, is determined in the quadratic approximation by the single force constant k_σ , so that for a linear dimer B...HX, for example,

$$k_\sigma = (16\pi^2 B_0^3 \mu / D_J)(1 - B_0/B_B - B_0/B_{\text{HX}}) \quad (2)$$

The corresponding expressions for molecules of different symmetry have also been given.¹⁶

The second measure of the strength of the hydrogen bond is the energy D_0 required to dissociate the ground-state dimer B...HX into B and HX. This quantity can be obtained by measuring the integrated intensity I of a ground-state rotational transition in each of B...HX, B, and HX in an equilibrium gas mixture of the three components.^{3,17-19} From the I values and the known rotational partition functions, the number densities $n_{0,0}(\text{B})$ etc. of the components in their $v = 0$, $J = 0$ states can be calculated. Simple statistical mechanical arguments¹⁸ then lead to the expression

$$n_{0,0}(\text{B}\cdots\text{HX})/n_{0,0}(\text{B})n_{0,0}(\text{HX}) = (h^2/2\pi\mu kT)^{3/2} \exp(D_0/RT) \quad (3)$$

¹⁶ D J Millen, *Can J Chem*, 1985, **63**, 1477

¹⁷ A C Legon, D J Millen, P J Mjoberg, and S C Rogers, *Chem Phys Lett*, 1978, **55**, 157

¹⁸ A C Legon, D J Millen, and H M North, *J Chem Phys*, 1987, **86**, 2530

¹⁹ A C Legon, D J Millen, and H M North, *Chem Phys Lett*, 1987, **135**, 303

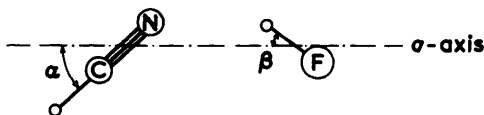


Figure 3 Definition of the instantaneous oscillation angles α and β of the HCN and HF subunits, respectively, in HCN...HF

so that D_0 is available from the equilibrium $n_{0,0}$ values (see Table 1).

C. Subunit Dynamics, Electric Charge Redistribution, Lengthening of the HF Bond from Nuclear Hyperfine Coupling Constants.—The nuclear hyperfine structure associated with the $J = 1 \leftarrow 0$ transition of $\text{HC}^{14}\text{N} \cdots \text{H}^{19}\text{F}$ shown in Figure 2 leads¹² to the ^{14}N -nuclear quadrupole coupling constant $\chi(^{14}\text{N})$ and the $\text{H}, ^{19}\text{F}$ nuclear spin–nuclear spin coupling constant D^{HF} . These quantities are reduced in magnitude from the HCN and HF free molecule values, respectively, as a result of the convolution of several effects.

First, even if the electric and geometric properties of HCN or HF were unaffected by the presence of the other subunit, an observed nuclear hyperfine coupling constant $C = \chi(^{14}\text{N})$ or D^{HF} in HCN...HF would be reduced from the free subunit value $C_0 = \chi_0(^{14}\text{N})$ or D_0^{HF} according to

$$C = \frac{1}{2}C_0 \langle 3\cos^2\theta - 1 \rangle \quad (4)$$

as a result of the zero-point angular oscillations of the subunits, where θ is the instantaneous angle α or β defined in Figure 3.

Secondly, however, account must be taken of the fact that, when the two subunits assume their equilibrium positions in the dimer, the electrical properties of each are affected by the presence of the other. Thus, the electric field gradient at the ^{14}N nucleus [to which $\chi(^{14}\text{N})$ is proportional] in $\text{HC}^{14}\text{N} \cdots \text{HF}$ differs from that in free HC^{14}N . The reason for this is the response^{20,21} of the electric charge distribution of HCN to the electric field and its derivatives at ^{14}N arising from the presence of the electric charge distribution of HF. This effect will be considered in much more detail in Section 4 when the Cl-nuclear quadrupole coupling constant^{22,23} of $(\text{CH}_3)_3\text{N} \cdots \text{HCl}$ is used as a probe of the extent of proton transfer from HCl to $(\text{CH}_3)_3\text{N}$.

Finally, the geometry of one subunit can be changed by the presence of the other. For example, in HCN...HF, the HF bond is lengthened by an amount $\delta r = 0.011 \text{ \AA}$ from the free molecule value.¹² Since D_0^{HF} is proportional $\langle r^{-3} \rangle_{0,0}$, where the average is over the zero-point motion, clearly the lengthening δr will

²⁰ A. C. Legon and D. J. Millen, *Proc. R. Soc. London, Ser. A*, 1988, **417**, 21.

²¹ J. Baker, A. D. Buckingham, P. W. Fowler, E. Steiner, P. Lazzaretti, and R. Zanasi, *J. Chem. Soc., Faraday Trans. 2*, 1986, **85**, 901.

²² A. C. Legon and C. A. Rego, *J. Chem. Phys.*, 1989, **90**, 6867.

²³ P. W. Fowler, A. C. Legon, C. A. Rego, and P. Tole, *Chem. Phys.*, 1989, **134**, 297.

make a contribution to the difference between D^{HF} of $\text{HCN} \cdots \text{HF}$ and D_0^{HF} of free HF.

Methods^{20,24-28} have been developed for deconvoluting the contributions to the changes in the free molecule nuclear hyperfine coupling constants *i.e.* for deconvoluting the effects of the angular oscillations of the subunits from those due to electrical and geometrical changes induced in one subunit by the other (see Section 4C). The results of applying these methods to $\text{HCN} \cdots \text{HF}$ are included in Table 1 where the operationally defined oscillation angles $\theta_{\text{av}} = \cos^{-1} \langle \cos \theta \rangle^{\frac{1}{2}}$, where $\theta = \alpha$ or β , and the HF bond lengthening δr so determined are given.¹²

D. Electric Charge Redistribution from the Stark Effect.—The application of a uniform static electric field to a gas of rotating molecules leads to a splitting of rotational energy levels and thus transitions (the Stark effect). When using a Stark-modulation microwave spectrometer, the Stark effect of a transition can be displayed simultaneously with the zero-field transition, as shown for the $J = 3 \leftarrow 2$ transition of $\text{HCN} \cdots \text{HF}$ in Figure 4. The downward pointing lobes constitute the Stark effect. The frequency displacement of a given M -lobe from the zero-field transition leads, by the application of standard methods,^{3,29} to the electric dipole moment μ of the linear dimer $\text{HCN} \cdots \text{HF}$. Given a model for the zero-point oscillation of the subunits (see Figure 3), μ for the dimer can be related to the electric dipole moments μ_{HCN} and μ_{HF} of the components by equation 5,

$$\mu = \mu_{\text{HCN}} \langle \cos \alpha \rangle + \mu_{\text{HF}} \langle \cos \beta \rangle + \Delta \mu \quad (5)$$

where $\Delta \mu$ is the enhancement of the electric dipole moment arising from polarization of one molecule by the other and from any charge transfer that occurs. Under the assumption that $\langle \cos \theta \rangle = \langle \cos^2 \theta \rangle^{\frac{1}{2}}$, where $\theta = \alpha$ or β , the value of $\Delta \mu$ given in Table 1 results.¹³

E. Vibrational Separations in the Hydrogen-bond Modes from Measurements on Vibrational Satellites.—Because of the weakness of the hydrogen-bond interaction, the intermolecular vibrational modes introduced on dimer formation are of low frequency. Consequently at the temperatures of ≈ 200 K used to observe the $J = 5 \leftarrow 4$ transition of $\text{HCN} \cdots \text{HF}$ by Stark-modulation microwave spectroscopy (Figure 1) a rich vibrational satellite pattern is evident. The satellites to high frequency of the ground-state transition are associated with the low-energy bending mode ν_{β} and those to low frequency with the stretching mode ν_{σ} . The forms of these modes are indicated schematically in Figure 1. By measuring the intensity of a satellite transition relative to that of the ground state, vibrational

²⁴ A. C. Legon and L. C. Willoughby, *Chem. Phys. Lett.*, 1984, **109**, 502.

²⁵ A. C. Legon and D. J. Millen, *Proc. R. Soc. London, Ser. A*, 1986, **404**, 89.

²⁶ P. Cope, D. J. Millen, and A. C. Legon, *J. Chem. Soc., Faraday Trans. 2*, 1986, **82**, 1189.

²⁷ P. Cope, D. J. Millen, L. C. Willoughby, and A. C. Legon, *J. Chem. Soc., Faraday Trans. 2*, 1986, **82**, 1197.

²⁸ A. C. Legon and D. J. Millen, *Chem. Phys. Lett.*, 1988, **144**, 136.

²⁹ A. C. Legon, D. J. Millen, and S. C. Rogers, *J. Mol. Spectrosc.*, 1978, **70**, 209.

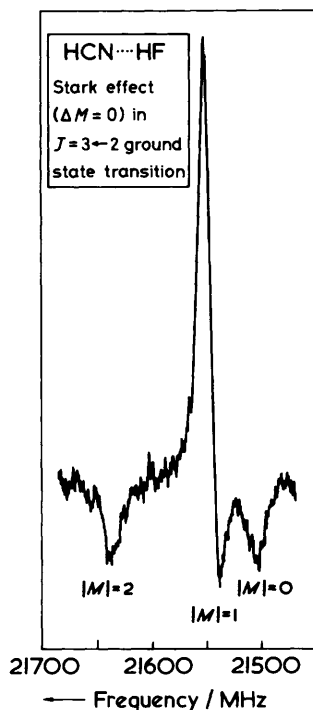


Figure 4 $J = 3 \leftarrow 2$ ground-state rotational transition of $\text{HC}^{14}\text{N}\cdots\text{HF}$ recorded with a Stark-modulation microwave spectrometer. The downward pointing lobes corresponds to the three $\Delta M = 0$ transitions into which the zero-field transition (upward pointing) splits in an applied uniform electric field of strength $\approx 1000 \text{ V cm}^{-1}$ (Redrawn from ref. 13 with permission of the American Chemical Society)

separations can be determined *via* the Boltzmann factor (assuming that the electric dipole transition moment is negligibly changed on vibrational excitation).³ Values for the separation $v = 1 \leftarrow 0$ in the modes ν_B and ν_σ so determined are included in Table 1. Note that, typically, the accuracy is only moderate.

The vibrational satellite associated with $\nu_B = 1$ is split into a doublet by the familiar *l*-doubling effect that is associated with a doubly degenerate bending mode of a linear molecule like $\text{HCN}\cdots\text{HF}$. The frequency splitting leads directly to the *l*-doubling constant ν_B which is related in the harmonic approximation to the vibrational frequencies ν_i of the molecule and the Coriolis coupling constants ζ_{Bi} by³⁰

$$q_B = (2B_c^2/\nu_B)[1 + 4\sum_i \zeta_{Bi}^2 \nu_i^2 / (\nu_i^2 - \nu_B^2)] \quad (6)$$

³⁰ C. H. Townes and A. L. Schawlow, 'Microwave Spectroscopy', McGraw-Hill, 1955, p. 33.

Use of equation 6 with the other (known) vibrational frequencies and the Coriolis coupling constants ζ_{Bi} (evaluated by standard techniques) leads to $\bar{\nu}_\beta = 72(4) \text{ cm}^{-1}$.³¹ This provides a route of useful accuracy to the lowest wavenumber bending mode which is difficult to characterize by other methods.

A detailed examination of the progression of vibrational satellites in Figure 1 associated with ν_β reveals perturbations of certain satellites from their expected frequency as a result of Fermi resonances that occur between levels $n\nu_\beta$ and $\nu_\sigma + (n - 2)\nu_\beta$. Analysis of the frequency shifts arising from such resonances³² leads to, for example, the wavenumber separation between the $\nu_\sigma = 1$ and $\nu_\beta = 2$ states of 16 cm^{-1} and to the cubic force constant $k_{\sigma\beta\beta}$ which appears in the matrix element responsible for coupling the states $\nu_\beta = 2$ and $\nu_\sigma = 1$.

4 Some Generalizations about the Properties of Dimers $B \cdots HX$

The summary in Section 3 reveals, by reference to the prototype dimer $\text{HCN} \cdots \text{HF}$, that a wide range of properties characterizing an isolated hydrogen-bonded dimer $B \cdots HX$ is available from investigations of its rotational spectrum. In fact, the rotational spectra of many dimers $B \cdots HX$ have now been examined (although not in as much detail as $\text{HCN} \cdots \text{HF}$). By a careful selection of series $B \cdots HX$ along which either B or HX is systematically varied, it has been possible to make some generalizations which have contributed to our understanding of the nature of the hydrogen bond. In this section several such generalizations are discussed. They fall into three categories which are concerned with: (A) the angular geometries of hydrogen-bonded dimers and some simple rules for their prediction; (B) an empirical relationship for predicting the strength of the hydrogen bond in dimers $B \cdots HX$ as measured by the intermolecular restoring force constant k_σ ; and (C) the position of the hydrogen atom in the hydrogen bond in the series $B \cdots \text{HF}$ as B is varied from weak to strong proton-acceptor molecules and in the series $(\text{CH}_3)_{3-n}\text{H}_n\text{N} \cdots \text{HX}$ as first n and secondly X is varied.

A. Angular Geometries of Hydrogen-bonded Dimers.—We begin by examining the observed angular geometries of four carefully chosen prototype dimers $B \cdots \text{HF}$, where $B = \text{H}_2\text{O}, \text{H}_2\text{S}, \text{H}_2\text{CO},$ and SO_2 .

A detailed analysis of the rotational spectrum of $\text{H}_2\text{O} \cdots \text{HF}$ led to the conclusions summarized in Figure 5. The lower part shows how the potential energy varies with the angle ϕ , where ϕ is the angle between the bisector of the $\text{H}\ddot{\text{O}}\text{H}$ angle and the $\text{O} \cdots \text{F}$ line, as defined in the figure. In the rotational spectrum of $\text{H}_2\text{O} \cdots \text{HF}$ each ground state transition is accompanied *inter alia* by a vibrational satellite series associated with the mode $\nu_{\beta(\text{O})}$, which is referred to as the out-of-plane bending mode even though in $\text{H}_2\text{O} \cdots \text{HF}$ it actually inverts the molecule from one nonplanar conformation (A), through the planar form, to the equivalent nonplanar arrangement (B) (see Figure 5). The intensities of the vibrational satellites associated with $\nu_{\beta(\text{O})}$ relative to that of the ground-state transition lead to vibrational separations in this mode (see Section 3) and these,

³¹ Z. Kisiel, A. C. Legon, D. J. Millen, and H. M. North, *Chem. Phys. Lett.*, 1986, **129**, 489.

³² A. C. Legon, D. J. Millen, and L. C. Willoughby, *Chem. Phys. Lett.*, 1987, **141**, 493.

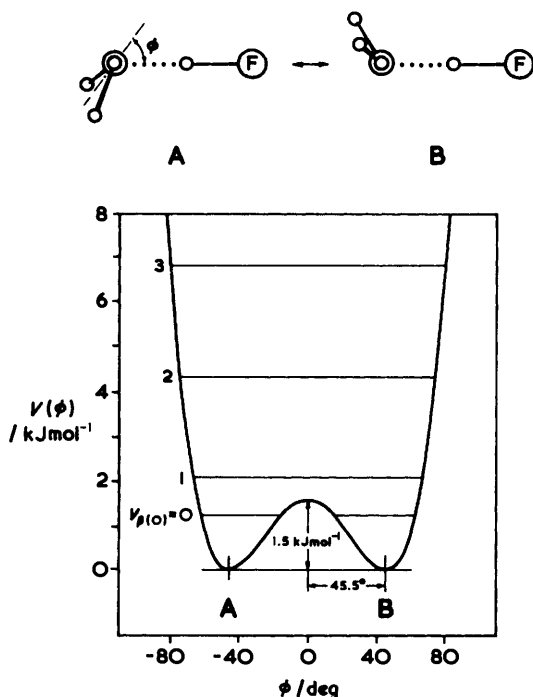


Figure 5 The experimentally determined one-dimensional potential energy function $V(\phi)$ for $\text{H}_2\text{O}\cdots\text{HF}$. The vibrational energy levels $v_{\text{B}(0)} = 0, 1, 2,$ and 3 associated with the out-of-plane bending mode $v_{\text{B}(0)}$ are indicated. The angle ϕ is defined in the diagram of the two equivalent equilibrium conformations **A** and **B** of $\text{H}_2\text{O}\cdots\text{HF}$

when taken in combination with the irregular frequency spacings of the satellites, can be used to generate the simple one-dimensional description of how the potential energy of the molecule varies with the angle ϕ shown in Figure 5.

The important conclusion from Figure 5 is that, although in the zero-point state the molecule is tunnelling with great facility between the two forms **A** and **B** so that the molecule can be described as *effectively planar*, the equilibrium geometry definitely has a *pyramidal configuration* about the oxygen atom. In particular, we note that the equilibrium value of the angle ϕ is quite close to one-half of the tetrahedral angle and that the barrier to the planar conformation ($\phi = 0$) is only 1.5 kJ mol^{-1} .

This observation about $\text{H}_2\text{O}\cdots\text{HF}$ suggests a very simple model for the dimer. In the equilibrium conformation the angular geometry can be understood if the HF molecule is envisaged to lie along the axis of a nonbonding (n) electron pair on oxygen, as conventionally drawn in the 'rabbit's ears' or 'water wings' representation and shown in Figure 6. The facile inversion between two equivalent, pyramidal forms can then be qualitatively understood.

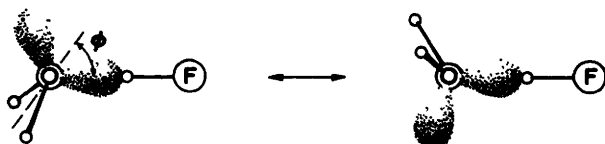


Figure 6 Models for the two equivalent equilibrium conformations of $\text{H}_2\text{O}\cdots\text{HF}$. The HF molecule is assumed to lie along the axis of a nonbonding electron (n) pair on H_2O . The n-pairs are drawn in the conventional 'rabbit's ears' representation.

(i) *The Rule for Angular Geometries when B carries Nonbonding Electron Pairs.* The above conclusion about the equilibrium geometry of $\text{H}_2\text{O}\cdots\text{HF}$ and other related results led to the proposal³³ of a simple rule for predicting the angular geometry of $\text{B}\cdots\text{HX}$ when B carries nonbonding electron pairs:

Rule (i): *The gas-phase equilibrium geometry of a hydrogen-bonded dimer $\text{B}\cdots\text{HX}$ can be obtained by assuming that the axis of the HX molecule coincides with the supposed axis of a nonbonding electron pair as conventionally envisaged.*

Evidently, this rule is electrostatic in origin if it is assumed that the positive end H of the HX molecule seeks out the direction of greatest electron density or nucleophilicity (the axis of the n-pair) on the molecule B. We next proceed to establish the validity of this rule by reference to the set of prototype dimers $\text{B}\cdots\text{HF}$ mentioned above. We shall discuss the question of the electrostatic nature of the rules and the existence or otherwise of nonbonding (n) electron pairs later.

The conventional model for the disposition of the eight valence electrons in H_2S is illustrated in Figure 7(a). The fact that the angle $\text{H}\hat{\text{S}}\text{H}$ is close to 90° is usually taken to imply involvement of $3p$ orbitals in the S–H bonds and sp hybrid orbitals for the n-pairs. The above rule therefore predicts a geometry for $\text{H}_2\text{S}\cdots\text{HF}$ in which HF lies perpendicular to the H_2S plane. The observed geometry³⁴ has the angle $\varphi = 89^\circ$, as shown in Figure 7(b). Moreover, unlike $\text{H}_2\text{O}\cdots\text{HF}$, there is no evidence from the ground-state rotational spectrum^{34,35} of inversion between the two equivalent n-pair positions. The accepted arrangement of the n-pairs on the oxygen atom in formaldehyde is of the sp^2 trigonal-type drawn in Figure 8(a) and leads to the predicted geometry illustrated there. The observed angular geometry [Figure 8(b)] is closely similar,³⁶ and again in the vibrational ground state there is no resolvable inversion splitting nor indeed is there in any of the observed vibrational satellites.³⁷

The three dimers $\text{H}_2\text{O}\cdots\text{HF}$, $\text{H}_2\text{S}\cdots\text{HF}$, and $\text{H}_2\text{CO}\cdots\text{HF}$ have been described by models of the molecule B in which the acceptor atom carries two

³³ A C Legon and D J Millen, *Discuss Faraday Soc*, 1982, 73, 71

³⁴ R Viswanathan and T R Dyke, *J Chem Phys*, 1982, 77, 1166

³⁵ L C Willoughby, A J Fillery-Travis, and A C Legon, *J Chem Phys*, 1984, 81, 20

³⁶ F A Baiocchi and W Klemperer, *J Chem Phys*, 1983, 78, 3509

³⁷ F J Lovas, R D Suenram, S Ross, and M Klobukowski, *J Mol Spectrosc*, 1987, 123, 167

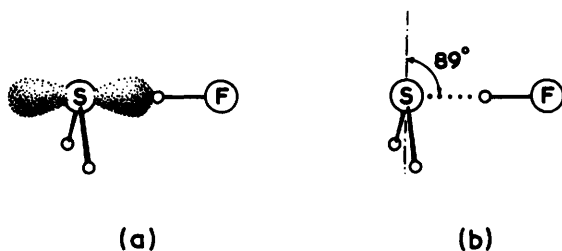


Figure 7 (a) The angular geometry of $\text{H}_2\text{S}\cdots\text{HF}$ predicted by using Rule (i) and the conventional nonbonding electron pair model of H_2S . (b) The observed angular geometry of $\text{H}_2\text{S}\cdots\text{HF}$

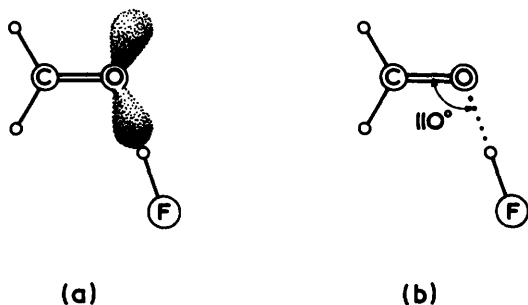


Figure 8 (a) The angular geometry of $\text{H}_2\text{CO}\cdots\text{HF}$ predicted by using Rule (i) and the conventional nonbonding electron pair model of H_2CO . (b) The observed angular geometry of $\text{H}_2\text{CO}\cdots\text{HF}$

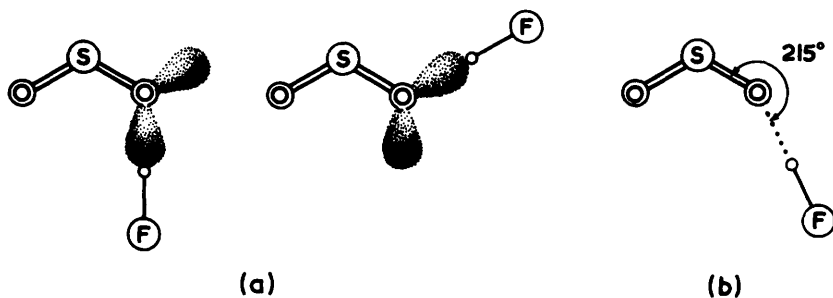


Figure 9 (a) The two possible angular geometries of $\text{SO}_2\cdots\text{HF}$ predicted by using Rule (i) and the conventional nonbonding electron pair model of SO_2 . The first has a cis arrangement with respect to the $\text{S}=\text{O}$ bond while the second has a trans arrangement. (b) The observed angular geometry of $\text{SO}_2\cdots\text{HF}$

equivalent n-pairs. As a further test of the rule, we now examine a case where the acceptor atom of B carries two *inequivalent* n-pairs. The prototype molecule here is SO_2 and is shown in Figure 9(a). Clearly, there is now the possibility,

according to the rule, of an angular geometry for $\text{SO}_2 \cdots \text{HF}$ in which HF completes either a *cis* or a *trans* arrangement with respect to the S=O double bond. The geometry of the isomer observed by pulsed-nozzle, FT microwave spectroscopy^{38,39} and presumably that of lowest energy is displayed in Figure 9(b) and clearly approximates more closely to the *cis* form.

Many of these molecules $\text{B} \cdots \text{HX}$ have angular geometries in good agreement with those predicted by the rule, *eg* $\text{HCN} \cdots \text{HF}$, $\text{OC} \cdots \text{HF}$, $(\text{HF})_2$, $\text{H}_3\text{N} \cdots \text{HCl}$, *etc* and have been discussed elsewhere⁴⁰⁻⁴¹

(ii) *What Happens When the Acceptor Molecule B Carries No Nonbonding Electron Pairs But Only π -Bonding Electron Pairs?* Some investigations carried out in 1980 at the University of Illinois shortly after the development of pulsed-nozzle, FT microwave spectroscopy centred on dimers $\text{B} \cdots \text{HCl}$ where B was ethyne,⁴² ethene,⁴³ and cyclopropane^{44,45}. As a result of this work it was possible to enunciate part (ii) of the rules for predicting angular geometries.³³

The Rules (ii): *The gas-phase equilibrium geometry of $\text{B} \cdots \text{HX}$ when B carries no n-pairs but only π -bonding pairs can be predicted by assuming that the axis of the HX molecule intersects the internuclear axis of the atoms forming the π -bond and is perpendicular to the plane of symmetry of the π -bond*

The conventional π -electron models of ethyne, ethene, and cyclopropane are drawn schematically in Figure 10(a) and the direction along which the HCl molecule is expected to lie according to the above rule is shown in each case. The model used for cyclopropane is that due to Coulson and Moffitt⁴⁶. They proposed that the C-C bond was formed by overlap of sp^3 hybrid orbitals on adjacent carbon atoms to produce a bent bond (*ie* where the line of greatest electron density does not coincide with the internuclear line). The pseudo- π character required by the much-invoked chemical analogy between cyclopropane and ethene is then readily understood. The general forms of the observed angular geometries⁴²⁻⁴⁵ are shown in Figure 10(b). Thus ethyne $\cdots \text{HCl}$ is T-shaped while HCl lies along the perpendicular C_2 axis of ethene and along the direction of a median of the cyclopropane equilateral triangle in cyclopropane $\cdots \text{HCl}$.

(iii) *What Happens When the Acceptor Molecule B Carries Both Nonbonding and π -Bonding Electron Pairs?* This situation was dealt with³³ by a third part to the rules enunciated in Section 4A(i) and (ii).

The Rules (iii): *When the acceptor molecule B carries both nonbonding and*

³⁸ A J Fillery-Travis and A C Legon, *Chem Phys Lett*, 1986, **123**, 4

³⁹ A J Fillery-Travis and A C Legon, *J Chem Phys*, 1986, **85**, 3180

⁴⁰ A C Legon and D J Millen, *Chem Soc Rev*, 1987, **16**, 467

⁴¹ A C Legon and D J Millen, *Acc Chem Res*, 1987, **20**, 39

⁴² A C Legon, P D Aldrich, and W H Flygare, *J Chem Phys*, 1981, **75**, 625

⁴³ P D Aldrich, A C Legon, and W H Flygare, *J Chem Phys*, 1981, **75**, 2126

⁴⁴ A C Legon, P D Aldrich, and W H Flygare, *J Am Chem Soc*, 1980, **102**, 7584

⁴⁵ A C Legon, P D Aldrich, and W H Flygare, *J Am Chem Soc*, 1982, **104**, 1486

⁴⁶ C A Coulson and W E Moffitt, *Philos Mag* 1949 **40**, 1

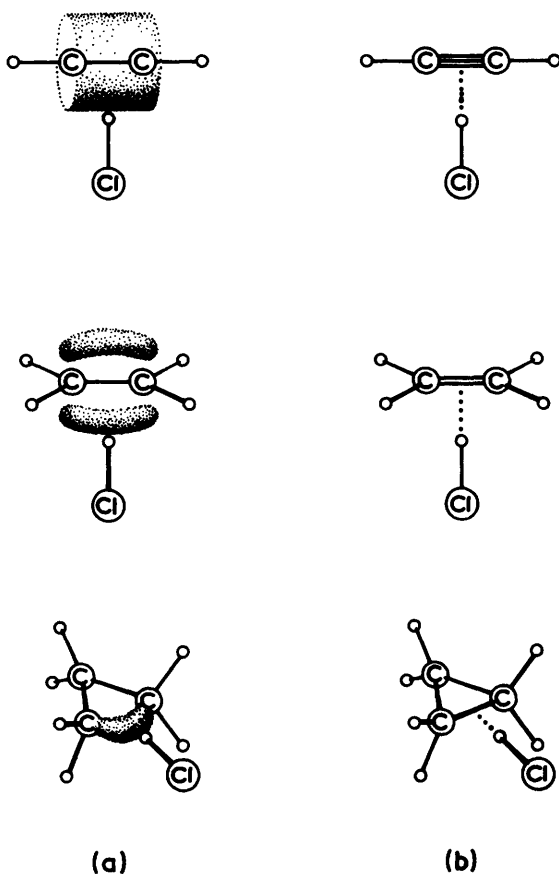


Figure 10 (a) The angular geometries of ethyne...HCl, ethene...HCl and cyclopropane...HCl predicted by using Rule (ii) with the π -bonding electron pair models of ethyne and ethene and the Coulson-Moffitt pseudo- π bonding electron pair model of cyclopropane. (b) The observed angular geometries of ethyne...HCl, ethene...HCl, and cyclopropane...HCl

π -bonding electron pairs, the nonbonding pairs dictate the angular geometry of B...HX.

There is ample evidence in favour of this part of the rules among molecules already mentioned. Thus in $\text{HCN}\cdots\text{HF}$, $\text{H}_2\text{CO}\cdots\text{HF}$, and $\text{SO}_2\cdots\text{HF}$ the angular geometry is as predicted by part (iii), with an n-pair acting as the nucleophile. Another interesting example that illustrates this is the observed angular geometry of the vinyl fluoride...HCl dimer shown in Figure 11. The dimer has all nuclei essentially coplanar, with the HCl molecule lying along a

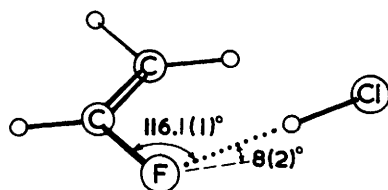


Figure 11 The observed angular geometry of the dimer formed between vinyl fluoride and hydrogen chloride. The hydrogen bond forms along the direction of a nonbonding electron pair on F rather than along the axis of the π -electron pair, i.e. rather than perpendicular to the C=C bond, as required by Rule (iii)

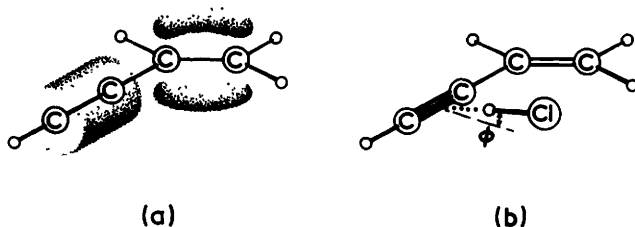


Figure 12 (a) Schematic diagram of the π -electron density in the planar molecule but-3-en-1-yne. (b) The observed angular geometry of the hydrogen-bonded dimer formed between but-3-en-1-yne and hydrogen chloride. The HCl axis lies perpendicular to the C \equiv C bond axis, displaced slightly (0.04 Å) towards the vinyl group but rotated out of the but-3-en-1-yne plane by the angle $\phi = 34^\circ$.

direction that makes a nearly tetrahedral angle with the C-F bond direction. This result again suggests that the n-pairs of fluorine rather than the π -pair dictate the geometry.⁴⁷

(iv) *What Happens When the Acceptor Molecule B Carries π -bonding Electron Pairs on Different Sites?* There are two ways in which an acceptor molecule B can carry π -bonding electrons on more than one site: the π bonds can be conjugated or cumulated. The prototype molecules in these classes are then but-3-en-1-yne and allene, respectively. Hydrogen-bonded dimers involving each of these acceptor molecules have been investigated recently.^{48,49} The π -bonding electron-pair model of but-3-en-1-yne is shown in Figure 12(a) while the observed geometry for its dimer with HCl is shown in Figure 12(b). Rule (ii) is of course non-committal about which π -bond the HCl molecule will prefer but when taken in combination with the intermolecular stretching force constants⁵⁰ $k_\sigma = 6.4$ and 5.9 N m^{-1} for B...HCl when B is ethyne and ethene, respectively, the observed arrangement can be readily rationalized. Nor does rule (ii) allow a prediction about the orientation of the HCl axis with respect to the plane of but-3-en-1-yne.

⁴⁷ Z Kisiel, P W Fowler, and A C Legon, *J Chem Phys.*, to be published

⁴⁸ Z Kisiel, P W Fowler, A C Legon, D Devanne, and P Dixneuf, *J Chem Phys.*, to be published

⁴⁹ A C Legon and L C Willoughby, *Chem Phys Lett*, 1988, **143**, 214

⁵⁰ Recalculated from the Δ_j values of refs 42 and 43 by the method of ref 16

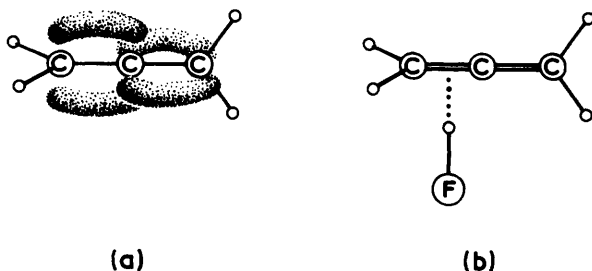


Figure 13 (a) Schematic diagram of the π -electron density in allene. (b) The observed angular geometry of the hydrogen-bonded dimer formed between allene and hydrogen fluoride. The HF axis is displaced by 0.126(9) Å from the midpoint of the C=C bond towards the central carbon atom

The quantitative electrostatic model of Buckingham and Fowler,⁵¹ on the other hand, not only predicts that the HCl subunit binds to the triple bond but also predicts the out-of-plane angle ϕ to be 27° , in excellent agreement with the experimental value of 34° .

The π -electron pair model of allene shown in Figure 13(a) suggests that the dimer of allene and HF should have an L-shaped geometry and that because of the cumulated nature of the bonds the H end of the HF molecule might move with facility from one of the four equivalent positions to another. These expectations are borne out in the experimental observations, as shown by the geometry in Figure 13(b) and by the signs of conformational nonrigidity exhibited in the rotational spectrum.⁴⁹

(v) *Is There Evidence for the Existence of Nonbonding Electron Pairs?* There is now evidence that the rules for predicting the angular geometries of hydrogen-bonded dimers are obeyed in the vast majority of cases where the experimental arrangement is known. It is of interest to ask in particular why the rules involving nonbonding electron pairs work, for the ‘rabbit’s ears’ representation of n-pairs is purely pictorial and conventional. Indeed, if the total electron density distribution around the oxygen atom in H₂O (as predicted from high quality *ab initio* SCF calculations⁵²) is examined, it is found to be essentially hemispherical, with little evidence of ‘ears’, as shown schematically in Figure 14. Is there any justification for the conventional representation of n-pairs? This question can be answered by examining the electrostatic potential as a function of angle near to the oxygen atom in H₂O.

Implicit in the Rules is the assumption of a simple electrostatic interaction of B and HX with no perturbation of their electric charge distributions. If we restrict attention to HF as the proton donor, it turns out that (as shown in Figure 14) its electric charge distribution can be represented⁵¹ in first approximation as having

⁵¹ A. D. Buckingham and P. W. Fowler, *Can. J. Chem.*, 1985, **63**, 2018.

⁵² See, for example, J. Bicerano, D. S. Marynik, and W. N. Lipscomb, *J. Am. Chem. Soc.*, 1978, **100**, 732.

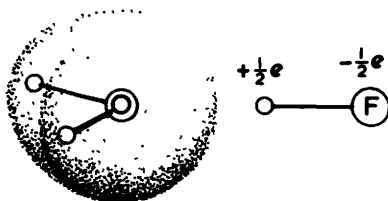


Figure 14 Schematic representation of the total electron density distribution obtained for the water molecule when using high quality *ab initio* SCF molecular orbital calculations. Also shown is a simple, approximate representation of the electrostatic charge distribution of hydrogen fluoride

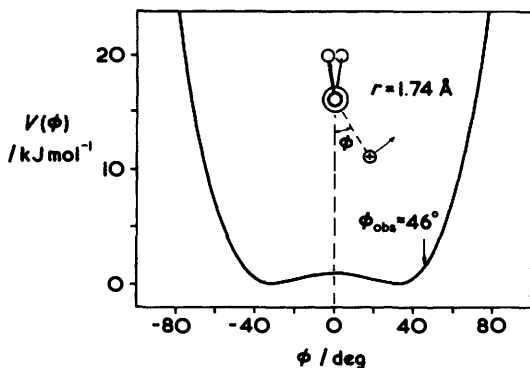


Figure 15 Variation of the electrostatic potential energy $V(\phi)$ of a charge $+e$ with the angle ϕ at a distance 1.74 \AA from the oxygen atom in H_2O . The angle ϕ lies in the plane perpendicular to the molecular plane and containing the nonbonding electron pair. The distance $r = 1.74 \text{ \AA}$ is equal to the experimental distance $r(\text{O} \cdots \text{H})$ in $\text{H}_2\text{O} \cdots \text{HF}$

residual charges of approximately $+0.5 e$ on H and $-0.5 e$ on F. Presumably, in the even cruder approximation (the zeroth) we might ignore the F end of HF in the interaction of B and HF and therefore assume that the positive charge on H seeks a position where its potential energy is a minimum. Thus, at this level of approximation, it might be better to examine how the electrostatic potential energy of a nonperturbing point positive charge varies with angle at an appropriate distance from B [e.g. the experimental distance $r(\text{B} \cdots \text{H})$].

Nowadays, the required electrostatic potential energy at a given distance from a molecule B can be calculated from a good *ab initio* SCF charge distribution by representing the latter through the distributed multipole analysis (DMA) due to Stone.⁵³ The DMA's used in the calculations discussed below are those generated by Buckingham and Fowler.⁵¹

Figure 15 shows the variation of the electrostatic potential energy $V(\phi)$ of a nonperturbing point protonic charge* with the angle ϕ in the n-pair plane of

⁵³ A J Stone, *Chem Phys Lett*, 1981, **83**, 233

* Strictly, to accord with the simple electrostatic model of HF in which charges of $0.54 e$ and $-0.54 e$ appear on H and F, respectively, the potential energies $V(\phi)$ etc should be multiplied by 0.54

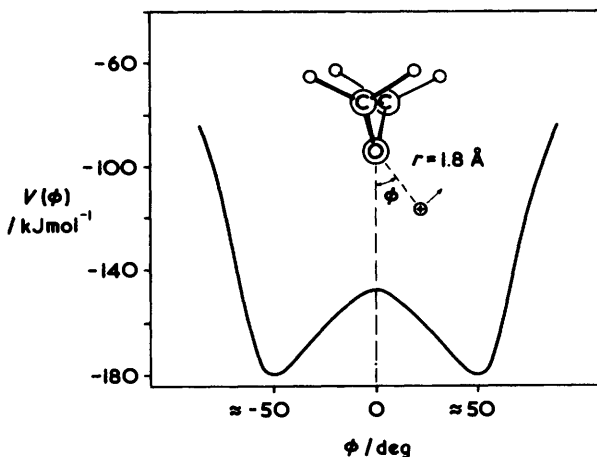


Figure 16 The variation of $V(\phi)$ with ϕ for oxirane. The angle ϕ has a definition similar to that given in the caption to Figure 15. The distance $r = 1.8 \text{ \AA}$ is approximately equal to the observed distance $r(\text{O} \cdots \text{H})$ in $(\text{CH}_2)_2\text{O} \cdots \text{HF}$ (Redrawn from Ref. 54 with permission of the American Institute of Physics)

H_2O at a distance r equal to the experimental distance⁷ $r(\text{O} \cdots \text{H}) = 1.74 \text{ \AA}$ of $\text{H}_2\text{O} \cdots \text{HF}$. We note the similarity of the curve so generated with that determined experimentally⁸ for inversion of $\text{H}_2\text{O} \cdots \text{HF}$ (see Figure 5), especially the two equivalent minima at angles close to those observed and the potential energy barrier of only a few kJ mol^{-1} . The corresponding curve for oxirane⁵⁴ shown in Figure 16 exhibits more widely separated minima and a higher barrier, as observed⁹ in oxirane $\cdots \text{HF}$ (see later). For H_2S , the minima occur at $\phi \approx \pm 80^\circ$ and the potential energy barrier to the planar form is high, as shown in Figure 17. Such a function is consistent with the conventional model of H_2S , the observed right-angled geometry of $\text{H}_2\text{S} \cdots \text{HF}$ (see Figure 7)³⁴ and with the fact that no inversion doubling is detected in the zero-point state.^{34,35} The form of the $V(\theta)$ versus θ curve generated when the nonperturbing point protonic charge is taken around the oxygen atom in formaldehyde in the plane of the molecule and at a distance $r = 1.79 \text{ \AA}$ [the experimental distance $r(\text{O} \cdots \text{H})$ in $\text{H}_2\text{CO} \cdots \text{HF}$]³⁶ is given in Figure 18, in which the angle θ is also defined. The shape of the curve is consistent semi-quantitatively with that of the one-dimensional potential energy function determined experimentally³⁷ for the corresponding low-frequency bending mode of $\text{H}_2\text{CO} \cdots \text{HF}$ which exhibits minima at $\theta = \pm 70^\circ$ and a barrier to the C_{2v} form of $\text{H}_2\text{CO} \cdots \text{HF}$ of approx. 5 kJ mol^{-1} . Finally, the calculated electrostatic potential energy $V(\theta)$ of a positive protonic charge taken around one of the oxygen atoms of SO_2 in the molecular plane (Figure 19) shows evidence not only of minima at angles in close agreement with those attributed to the *cis* and *trans* nonbonding electron pairs of SO_2 (see

⁵⁴ R. Bonaccorsi, E. Scrocco, and J. Tomasi, *J. Chem. Phys.*, 1970, **52**, 5270.

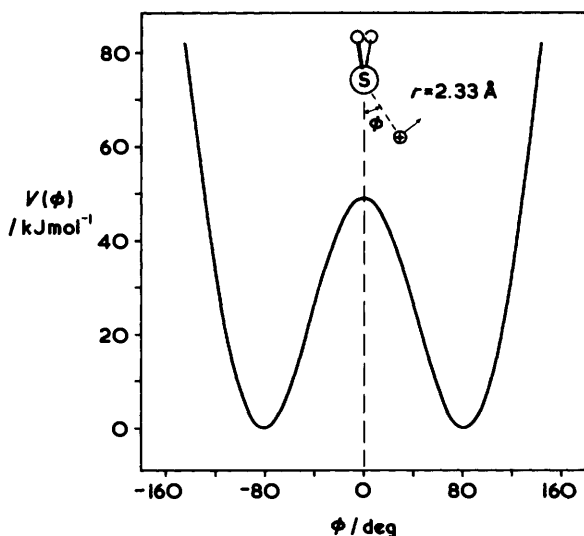


Figure 17 Variation of the electrostatic potential energy $V(\phi)$ of a charge $+e$ with the angle ϕ at a distance of 2.33 \AA from the sulphur atom in H_2S . The angle ϕ is defined in the plane perpendicular to the H_2S plane as indicated. The distance $r = 2.33 \text{ \AA}$ is equal to the experimental distance $r(\text{S} \cdots \text{H})$ in $\text{H}_2\text{S} \cdots \text{HF}$.

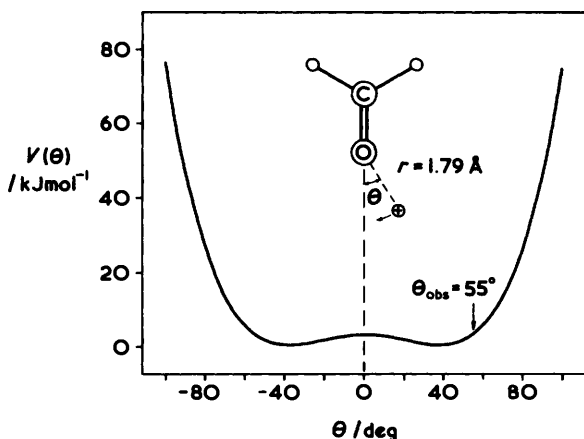


Figure 18 Variation of the electrostatic potential energy $V(\theta)$ of a charge $+e$ with the angle θ at a distance 1.79 \AA from the oxygen atom of H_2CO . The charge $+e$ is confined to the molecular plane and θ is defined as indicated. The distance $r = 1.79 \text{ \AA}$ is equal to the experimental distance $r(\text{O} \cdots \text{H})$ in $\text{H}_2\text{CO} \cdots \text{HF}$.

Figure 9) but also, in agreement with the experimental observation for $\text{SO}_2 \cdots \text{HF}$, that the *cis* pair corresponds to the lowest energy^{38 39}

In each of the cases investigated (Figures 15 to 19) we observe that the

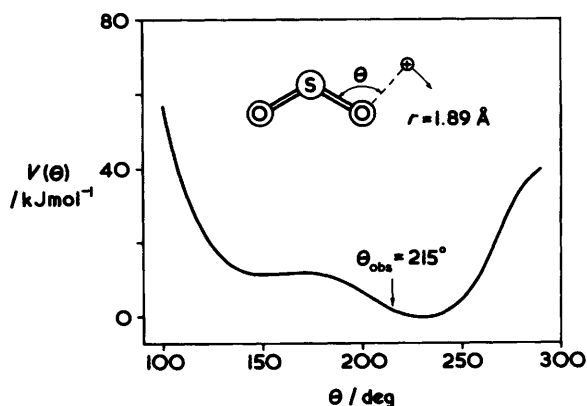


Figure 19 Variation of the electrostatic potential energy $V(\theta)$ of a charge $+e$ with the angle θ at a distance $r = 1.89 \text{ \AA}$ from one of the oxygen atoms in SO_2 . The charge $+e$ is confined to the molecular plane and θ is defined as indicated. The distance $r = 1.89 \text{ \AA}$ is equal to the experimental distance $r(\text{O} \cdots \text{H})$ in $\text{SO}_2 \cdots \text{HF}$

electrostatic potential energy of a point positive charge has minima at approximately those angles that conventionally would be associated with the directions of nonbonding electron pairs. Given that the electric charge distribution of B has been accurately represented when calculating the electrostatic potential energy of $+e$, these diagrams present strong evidence for the existence of nonbonding electron pairs, if not in the conventional 'rabbit's ears' sense, then at least with respect to their influence in determining the angular geometry of hydrogen-bonded dimers $\text{B} \cdots \text{HF}$. In fact, if we move from the zeroth order approximation, treat the HF molecule as an extended electric dipole with charges of $0.54 e$ and $-0.54 e$ on H and F, respectively, and calculate the variation of electrostatic potential energy of this dipole with angle in a similar manner, the above conclusions are reinforced. In general, the minima occur at positions even closer to those conventionally associated with n-pairs, as shown for $\text{H}_2\text{CO} \cdots \text{HF}$ in Figure 20 where the potential energy curve thereby generated is compared with the experimental function for the low-frequency bending mode of the dimer determined by Lovas *et al.*³⁷ The agreement between the calculated and experimental functions is remarkable.

The above simple electrostatic analysis has been used to discuss the reasons why the empirical rules based on nonbonding electron pairs are useful for predicting angular geometries. More complete electrostatic models, in which fuller representations of the electric charge distribution of the HX molecule are used and the minimum in electrostatic energy found, have preceded the analysis given here.^{51,55} That due to Buckingham and Fowler⁵¹ has been particularly successful for a wide range of dimers (hydrogen-bonded or otherwise).

⁵⁵ J T Brobjer and J. N. Murrell, *J. Chem. Soc., Faraday Trans. 2*, 1982, **78**, 1853; 1983, **79**, 1455.

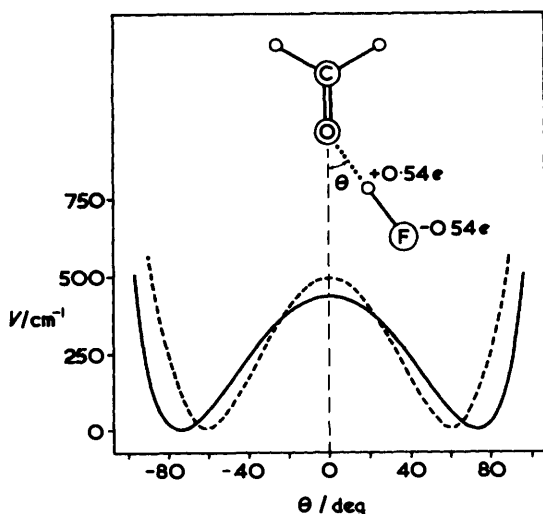


Figure 20 Variation of the potential energy $V(\theta)$ with θ in $\text{H}_2\text{CO}\cdots\text{HF}$. The solid line is the potential energy function governing the low frequency intermolecular bending mode determined experimentally by Lovas et al (Ref 37). The dotted curve plots out as a function of θ the electrostatic potential energy $V(\theta)$ of the HF molecule when it lies along the line defining the angle θ in Figure 18 as measured from the C_2 axis of H_2CO . The HF molecule is treated as a simple extended electric dipole with charges of $+0.54 e$ on H and $-0.54 e$ on F. The H and F atoms of hydrogen fluoride are maintained at the distances from the oxygen atom found experimentally in $\text{H}_2\text{CO}\cdots\text{HF}$. (See caption to Figure 18 and text)

(vi) *A Simple Corollary of the Rules* The rules and the electrostatic interpretation of the existence of nonbonding electron pairs discussed in Sections 4A(iv) and (v) suggest that, as long as the interaction between B and an HF molecule is sufficiently weak that both subunit electric charge distributions are essentially unperturbed, the HF molecule will lie at equilibrium along the axis of a nonbonding electron pair, as conventionally pictured. In other words, the HF molecule acts as a probe for the directions of n-pairs. This corollary has been tested by considering the series of molecules 2,5-dihydrofuran,⁵⁶ oxetane,⁵⁷ and oxirane,⁵⁸ as illustrated in Figure 21. Along the series the angle $\text{C}\ddot{\text{O}}\text{C}$ decreases, thereby implying that the angle between the n-pairs on oxygen opens up commensurately. The angular geometries of the corresponding series of hydrogen-bonded dimers $\text{B}\cdots\text{HF}$ have been experimentally established,^{59 10 9} with the results summarized in Figure 22. The increase in the angle ϕ along the series does indeed suggest that the inter n-pair angle increases in the expected way.

⁵⁶ G. G. Engerholm, Dissertation, University of California Berkeley California *Disc Abstr.* 1966 26 66-3580

⁵⁷ S. I. Chan, J. Zinn, J. Fernandez, and W. D. Gwinn *J. Chem. Phys.* 1960, 33 1643; 1961 34 1319

⁵⁸ C. Hirose, *Bull. Chem. Soc. Jpn.*, 1974 47, 976 and 1311

⁵⁹ R. A. Collins, D. J. Millen, and A. C. Legon *J. Mol. Struct.* 1987 162 31

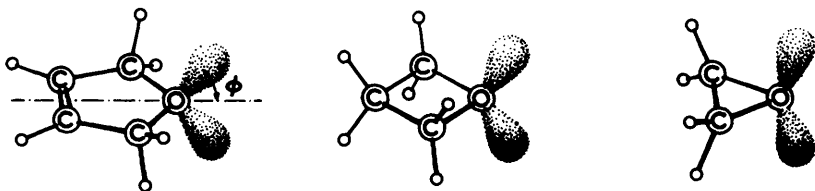


Figure 21 The conventional nonbonding electron pair models of 2,5-dihydrofuran, oxetane and oxirane. The internal ring angle COC decreases from 114.4° , through 91.9° to 61.6° along this series. It is assumed that the angle 2ϕ between the nonbonding electron pairs increases commensurately

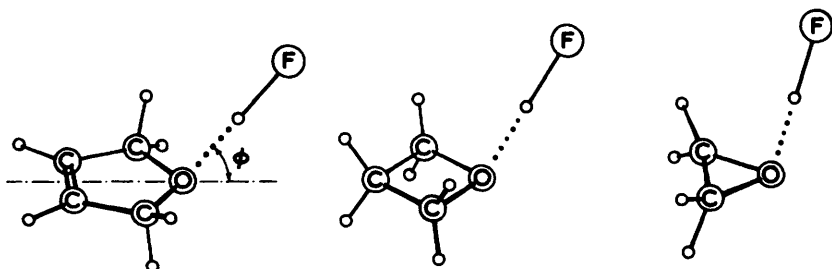


Figure 22 The experimentally determined angular geometries of a series of dimers $\text{B} \cdots \text{HF}$, where $\text{B} = 2,5\text{-dihydrofuran, oxetane, and oxirane}$. The angle ϕ increases from 48.5° through 57.9° to 71.8° along this series. If the HF molecule acts as a probe for the direction of a nonbonding electron pair on oxygen in each case, the increase in the angle 2ϕ between the nonbonding electron pairs predicted in the caption to Figure 21 is established

(vii) *The Rules and the Limit of Long/Weak Hydrogen Bonds.* Another consequence of the simple electrostatic interpretation of the Rules given in Section 4A(v) concerns the angular geometry that is predicted in the limit of a long, weak hydrogen bond in a dimer $\text{B} \cdots \text{HX}$. Presumably, the directing effects of n -pairs become less dominating as the hydrogen bond becomes weaker. This statement can be illustrated by considering how the depth and separation of the electrostatic potential energy minima discussed in Section 4A(v) vary with the distance r of the nonperturbing point positive charge e from the acceptor atom of B . Figure 23 illustrates how the potential energy curve for formaldehyde given in Figure 18 varies as r is varied. As expected, at short r the minima attributed to the directions of the conventional n -pairs at $\theta = \pm 60^\circ$ are deep but the potential energy maximum at $\theta = 0$ rapidly diminishes as r increases until at $r = 2.0 \text{ \AA}$ only a flat single minimum is evident.

This rapid loss of directing power of n -pairs can be tested experimentally. In general, the distance $r(\text{B} \cdots \text{H})$ increases and the hydrogen-bond strength decreases along a series $\text{B} \cdots \text{HF}$, $\text{B} \cdots \text{HCl}$, and $\text{B} \cdots \text{HCN}$.⁶⁰ The experimental

⁶⁰ See, for example, Table 12 in A. J. Fillery-Travis, A. C. Legon, and L. C. Willoughby, *Proc. R. Soc. London, Ser. A*, 1984, **396**, 405 which compares the distances $r(\text{Y} \cdots \text{X})$ and the k_σ values for $\text{H}_2\text{Y} \cdots \text{HX}$ where $\text{Y} = \text{O}$ or S and $\text{X} = \text{F, Cl, and CN}$.

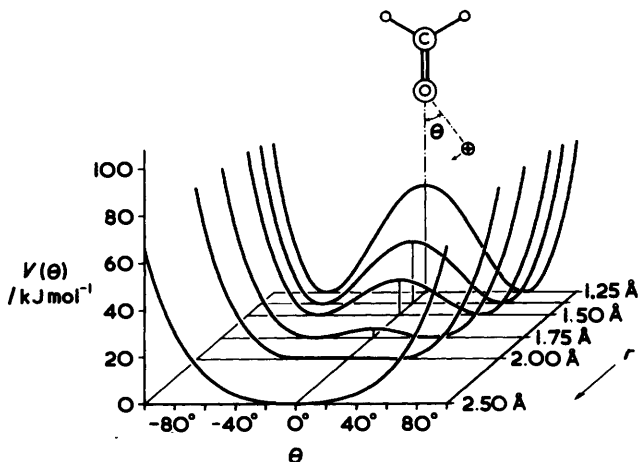


Figure 23 A series of electrostatic potential energy curves $V(\theta)$ for H_2CO of the type defined in Figure 18. Each curve corresponds to a different distance r of the charge $+e$ from the oxygen atom of H_2CO . As r increases the value of the maximum in the potential energy curve at the angle $\theta = 0^\circ$ rapidly decreases and even at distances as short as 2 Å the curve has only a single minimum

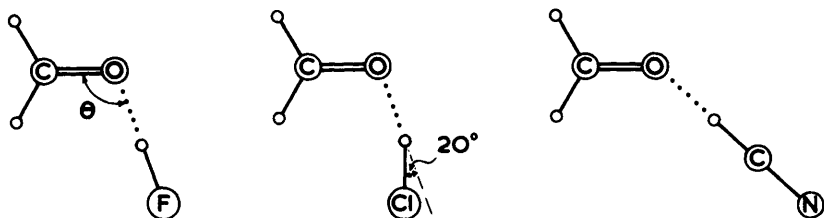


Figure 24 Experimental angular geometries of dimers $\text{H}_2\text{CO} \cdots \text{HX}$, where $\text{X} = \text{F}, \text{Cl},$ and CN . The angle θ is approx. 110° for the first two members of the series but for $\text{H}_2\text{CO} \cdots \text{HCN}$ has increased to 138° and there is spectroscopic evidence (see text) to suggest that the zero-point vibrational wavefunction has C_{2v} symmetry in this case

angular geometries,^{36,61,62} when $\text{B} = \text{H}_2\text{CO}$ are displayed in Figure 24. In the case of $\text{H}_2\text{CO} \cdots \text{HCN}$,⁶¹ the angle $180 - \theta$ is reduced to 42° from its value of 70° in $\text{H}_2\text{CO} \cdots \text{HF}$.³⁶ We note also that there is some evidence of a secondary hydrogen-bond interaction between Cl and a CH_2 hydrogen atom in $\text{H}_2\text{CO} \cdots \text{HCl}$ ⁶¹ (see below for further evidence of secondary hydrogen bonds). A similar effect to that in the $\text{H}_2\text{CO} \cdots \text{HX}$ series is discernible in the experimental angular geometries for $(\text{CH}_2)_2\text{O} \cdots \text{HX}$, where $\text{X} = \text{F},$ ⁹ $\text{Cl},$ ¹⁴ and $\text{CN},$ ⁶³ shown in Figure 25. While the angle $\varphi \approx 75^\circ$ when $\text{X} = \text{F}$ or Cl and there is no evidence for inversion doubling,^{9,14} the weaker, longer hydrogen bond when

⁶¹ G. T. Fraser, C. W. Gillies, J. Zozom, F. J. Lovas, and R. D. Suenram, *J. Mol. Spectrosc.*, 1987, **126**, 200.

⁶² E. J. Goodwin and A. C. Legon, *J. Chem. Phys.*, 1987, **87**, 2426.

⁶³ E. J. Goodwin, A. C. Legon, and D. J. Millen, *J. Chem. Phys.*, 1986, **85**, 676.

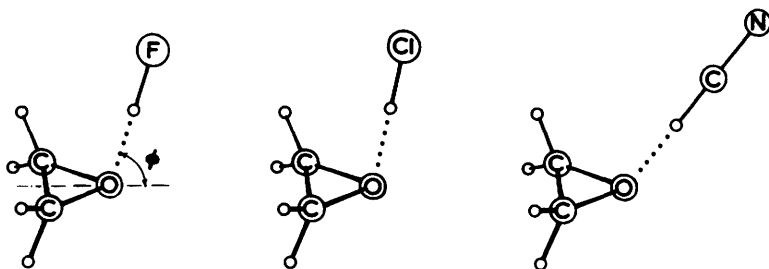


Figure 25 Experimental angular geometries of dimers $(\text{CH}_2)_2\text{O}\cdots\text{HX}$, where $\text{X} = \text{F}$, Cl , and CN . The angle φ has the values 72.6° , 78° , and 52° , respectively, for these dimers. The rotational spectrum in the case $\text{X} = \text{CN}$ exhibits inversion doubling and demonstrates that the vibrational wavefunctions have C_{2v} symmetry

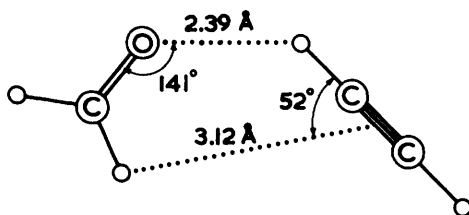


Figure 26 Experimental angular geometry of the dimer formed by formaldehyde and ethyne. The molecule is planar and unexpectedly rigid, presumably as a result of the secondary hydrogen bond formed by an H atom of H_2CO with the π bond of ethyne

$\text{X} = \text{CN}$ allows inversion of the HCN molecule between the two equivalent n -pairs on oxygen (as demonstrated by inversion doubling in the rotational spectrum),⁶³ presumably as a result of a lower potential energy barrier to the C_{2v} conformation. Consequently, the zero-point vibrational wavefunction of the molecule has C_{2v} symmetry and the angle φ obtained by fitting ground-state rotational constants is reduced to 52° .

(viii) *Secondary Hydrogen Bonds*. In general, a molecule B will consist of at least one nucleophilic region and at least one electrophilic region. The same applies to the molecule HX . Presumably, for a series $\text{B}\cdots\text{HX}$ in which B is fixed and HX varies from the strongest to the weakest proton donor (or electrophile) the primary hydrogen-bond interaction will become sufficiently weak that additional stability can be achieved by forming a secondary interaction (involving the nucleophilic centre of HX and the electrophilic centre of B) at the expense of distortion of the primary interaction from its energetically most favoured arrangement. This effect is evident in the series $\text{H}_2\text{CO}\cdots\text{HX}$. When HX is ethyne, the $\text{O}\cdots\text{HCCH}$ hydrogen bond is sufficiently weak that a secondary hydrogen bond to the π -bond of ethyne is forged through an H of H_2CO , as illustrated by the experimental angular geometry⁶⁴ in Figure 26. This dimer is

⁶⁴ N. W. Howard and A. C. Legon, *J. Chem. Phys.*, 1988, **88**, 6793.

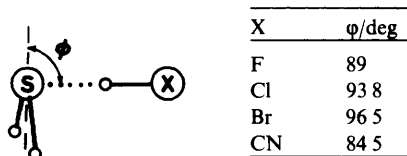


Figure 27 Evidence of the increasing importance of secondary hydrogen bonds along the series of dimers $\text{H}_2\text{S}\cdots\text{HX}$ where $\text{X} = \text{F}, \text{Cl},$ and Br . The secondary interaction between the H atom of H_2S and the halogen is demonstrated by the increasing angle ϕ as X is changed from F to Cl to Br. Evidently, the secondary interaction is unimportant when $\text{X} = \text{CN}$.

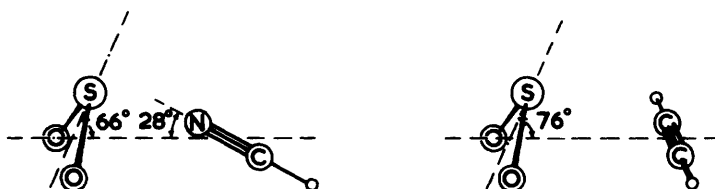


Figure 28 The observed angular geometries of the dimers formed by sulphur dioxide with hydrogen cyanide and with ethyne.

planar, cyclic, and unexpectedly rigid compared with $\text{H}_2\text{CO}\cdots\text{HCN}$. The original expectation, based on an extrapolation of the series shown in Figure 24 to $\text{HX} = \text{ethyne}$, was of a weak complex of C_{2v} symmetry and a linear $\text{CO}\cdots\text{HCCH}$ chain.

Further evidence of secondary hydrogen bonds can be discerned from the experimental angular geometries in the series of dimers $\text{H}_2\text{S}\cdots\text{HX}$ ($\text{X} = \text{F},^{34} \text{Cl},^{65} \text{Br},^{67} \text{CN}^{66}$) given in Figure 27. As X changes from F to Cl to Br the angle ϕ increases beyond 90° , presumably as a result of the increased ease of bending the hydrogen bond which then allows the secondary $\text{S}-\text{H}\cdots\text{X}$ interaction to come into play. For $\text{X} = \text{CN}$, the secondary interaction appears to be less important so that the tendency of the angle ϕ to approach $\phi = 0$ in the weak limit of the hydrogen bond is beginning to be observed (*i.e.* $\phi = 84^\circ$).

(ix) *Nonhydrogen-bond Interactions.* When the molecule B is not as simple as the prototype acceptors $\text{H}_2\text{O}, \text{H}_2\text{S}, \text{H}_2\text{CO}$, the interaction of B and HX need not be of the hydrogen-bonded type. As mentioned in (viii) above, each of B and HX is amphiphilic. Presumably, the interaction between the nucleophilic region of HX and the electrophilic region of B can predominate over the more usual interaction, especially if HX is rather a poor proton donor such as HCN or HCCH. This effect is clearly demonstrated in the experimentally determined angular geometries of the dimers $\text{B}\cdots\text{HCN}^{68}$ and $\text{B}\cdots\text{HCCH}^{69}$ when B is

⁶⁵ E J Goodwin and A C Legon, *J Chem Soc, Faraday Trans 2*, 1984, **80**, 51

⁶⁶ E J Goodwin and A C Legon, *J Chem Soc, Faraday Trans 2*, 1984, **80**, 1669

⁶⁷ A I Jaman and A C Legon, *J Mol Struct*, 1986, **145**, 261

⁶⁸ E J Goodwin and A C Legon, *J Chem Phys*, 1986, **85**, 6828

⁶⁹ A M Andrews, K W Hillig II, R L Kuczowski, N W Howard, and A C Legon, to be published

SO₂, as shown in Figure 28. Now neither the *cis*- or *trans*-hydrogen bonded forms suggested by the Rules (see Figure 9) is observed. Instead, the region near to S and perpendicular to the SO₂ plane is the electrophile and the n-pair on HCN or the π -pair of ethyne are the nucleophiles.

B. The Strength of the Hydrogen Bond in Dimers B...HX.—A desirable objective in obtaining an understanding of the hydrogen bond is to be able to predict its strength in a dimer B...HX from the properties of the component molecules B and HX. As discussed in Section 3, the strength of the hydrogen bond can be measured either by the hydrogen-bond stretching force constant k_{σ} or the zero-point dissociation energy D_0 . Although D_0 is available for only a few dimers, k_{σ} has been determined for a wide variety of species B...HX from centrifugal distortion constants (see Section 3). A comparison of k_{σ} within a series B...HX in which, say, HX is systematically varied while B is held constant gives a measure of the relative strength of the hydrogen bond along the series. When k_{σ} values are examined in this manner for B...HX that are not too strongly bound (*i.e.* where the interaction between the components can be described without invoking significant charge redistribution within each component or between the components) it is found⁷⁰ that there is a simple relationship among them. In fact, k_{σ} can be expressed by the empirical equation 7,

$$k_{\sigma} = cEN \quad (7)$$

where E and N are numbers associated with the molecules HX and B, respectively, and c is a constant having the value 0.25 N m^{-1} .

The success of the rules for predicting angular geometries (see Section 4A above) and of the quantitative electrostatic model developed by Buckingham and Fowler⁵¹ encourages a view of the hydrogen bond in which the interaction between B and HX is of the simple electrostatic type involving essentially unperturbed electric charge distributions, with the most electrophilic site on HX (*i.e.* the H atom) seeking the most nucleophilic site on B but with sites of the same philicity avoiding each other. For these reasons the quantities E and N have been called⁷⁰ *limiting, gas-phase electrophilicities* and *nucleophilicities*, respectively, the adjectives emphasizing that equation 7 applies only in the limit of weak interaction between a pair of molecules HX and B in isolation. The values of E and N assigned to six molecules HX and twelve molecules B, respectively, are collected together in Table 2. In combination with equation 7, Table 2 can be used to predict k_{σ} for a large number of dimers B...HX, including many values of k_{σ} not used in the original determination of E and N . We shall see later, however, that for certain combinations of B and HX [for example (CH₃)₃N...HCl and (CH₃)₃N...HBr] the k_{σ} values so predicted are very much smaller than those observed. In such cases, the disparity between $k_{\sigma}(\text{obs})$ and $k_{\sigma}(\text{calc})$ will be used as evidence that the dimers are not of the simple

⁷⁰ A. C. Legon and D. J. Millen, *J. Am. Chem. Soc.*, 1987, **109**, 356.

The Properties of Hydrogen-bonded Dimers from Rotational Spectroscopy

Table 2 Limiting, gas-phase nucleophilicities (*N*) and electrophilicities (*E*) of some molecules **B** and **HX**

Molecule B	<i>N</i>	Molecule HX	<i>E</i>
N ₂	2.2	HF	10.0
CO	3.4	HCl	5.0
PH ₃	4.4	HCN	4.25
H ₂ C=CH ₂ ^a	4.7	HBr	4.2
H ₂ S	4.8	HC≡CH	2.4
HC≡CH ^a	5.1	HCF ₃	1.9
(CH ₂) ₃ ^a	6.4		
HCN	7.3		
CH ₃ CN	8.1		
H ₂ O	10.0		
NH ₃	11.5		
(CH ₃) ₃ N ^b	14.8		

^a Values of *N* for HC≡CH, CH₂=CH₂, and (CH₂)₃ are given in A C Legon and D J Millen, *J Chem Soc, Chem Commun*, 1987, 987. Except for (CH₃)₃N (see footnote *b*), the remainder are taken from Ref 70. ^b Mean of the two values of *N* calculated from equation 7 using the *k_s* values of (CH₃)₃N...HF and (CH₃)₃N...HCN given in Refs 84 and 85, respectively.

hydrogen-bonded type and that significant proton transfer from HX to **B** must then be invoked.

C. Lengthening of the HX Bond on Formation of B...HX and the Question of Proton Transfer.—The empirical rules, discussed above, for predicting angular geometries of hydrogen-bonded B...HX rely implicitly on the notion that the simple electrostatic interaction of the subunits determines the relative orientation of minimum energy. No account is taken of mutual geometrical or electrical perturbation. This notion also figured in the discussion of the empirical equation 7 for predicting *k_s* values. In particular, the question of the extent of proton transfer from HX to **B**, important for a complete understanding of the nature of the hydrogen bond, was not considered.

Experimentally, the extent of proton transfer (*i.e.* the lengthening of the HX bond on formation of B...HX) is difficult to measure by conventional methods. The contribution of the H atom to the moments of inertia of B...HX is inevitably small because of its proximity to the centre of mass. Consequently, there is no hope of accurate location of this atom from the changes in *zero-point* moments of inertia on D/H substitution and we must appeal to other methods. Although not useful in this context, such changes in moments of inertia have been used, however, to show for extended series of dimers B...H(D)X that the distance *r*(B...X) shortens systematically on D/H substitution.⁷¹

In this section, we first discuss the lengthening δr of the HF molecule when incorporated into B...HF. The source of δr is the H,F nuclear spin-nuclear spin coupling constant *D*^{HF} in combination with the D-nuclear quadrupole

⁷¹ A C Legon and D J Millen, *Chem Phys Lett*, 1988, **147**, 484

coupling constant $\chi(D)$. We shall show that δr is small even for strongly bound dimers $B \cdots HF$ and that a simple electrostatic model accounts for the magnitude of δr . Finally, we consider how, by progressively increasing the proton affinity of B and the ease of distortion of HX , dimers in which the extent of proton transfer is significant can be investigated. In particular, we show experimentally that for the series $(CH_3)_{3-n}H_nN \cdots HX$ variation of n from 3 to 0 and X from F through Cl to Br leads to the identification of an ion pair $(CH_3)_3NH^+ Br^-$ in the vapour phase.

(i) *Dimers $B \cdots HF$ and the Lengthening δr of the HF Bond.* When the rotational spectrum of a dimer $B \cdots HF$ is observed by pulsed-nozzle, Fourier-transform microwave spectroscopy, hyperfine structure arising from H,F nuclear spin-nuclear spin coupling can be resolved and the corresponding coupling constant(s) determined. As indicated in Section 3C, in the free HF molecule the observed zero-point coupling constant D_0^{HF} is simply related to the internuclear distance r by

$$D_0^{HF} \propto \langle r^{-3} \rangle_{HF} \quad (8)$$

where the constant of proportionality contains only the H and F nuclear magnetic moments and other physical constants.⁷² The average is over the HF zero-point motion. Now consider that an axially symmetric dimer $B \cdots HF$ is formed in the hypothetical state in which all other contributions to the zero-point motion but the HF stretching motion are quenched. The appropriate coupling constant for this hypothetical molecule is then given by equation 9

$$D_{zz}^{HF} \propto \langle r^{-3} \rangle_{HF} \quad (9)$$

where the angular brackets signify again the average over the HF stretching motion (along the symmetry axis of the axially symmetric dimer $B \cdots HF$) but as modified by dimer formation. Equations 8 and 9 then allow the operational definitions of HF bond lengths $r_0 = \langle r^{-3} \rangle_{HF}^{-1/3}$ and $r_0 + \delta r = \langle r^{-3} \rangle_{HF}^{-1/3}$, the second of these taking account of the fact that the average is with respect to an extended HF bond. Clearly, D_{zz}^{HF} and D_0^{HF} allow an estimate of δr .

But D_{zz}^{HF} is not an observable. Of course, the observed coupling constant D^{HF} of the axially symmetric species $B \cdots HX$ is the full zero-point expectation value, to which the contribution of the angular oscillation of the type defined by β in Figure 3 is by far the most important. Then a good approximation to D_{zz}^{HF} can be obtained from the expression

$$D^{HF} = \frac{1}{2} D_{zz}^{HF} \langle 3\cos^2\beta - 1 \rangle \quad (10)$$

where now the angular brackets denote the average over the contribution of the

⁷² W. G. Read and W. H. Flygare, *J. Chem. Phys.*, 1982, **76**, 2238.

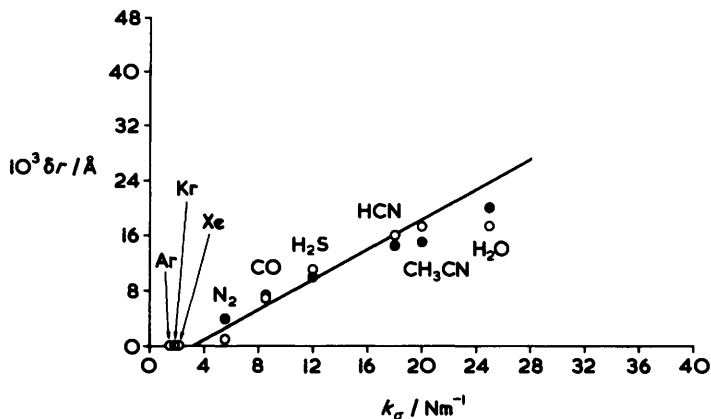


Figure 29 Variation of the lengthening δr of the HF molecule on formation of $B \cdots HF$ with hydrogen bond stretching force constant k_σ for $B = \text{Ar, Kr, Xe, N}_2, \text{CO, H}_2\text{S, HCN, CH}_3\text{CN and H}_2\text{O}$. \circ , Experimental values. \bullet , Calculated from a simple electrostatic model of $B \cdots HF$ (see text)

angular oscillation to the zero-point motion and δr is assumed independent of β . A method has been proposed²⁵ which allows $\beta_{av} = \cos^{-1} \langle \cos^2 \beta \rangle^{1/2}$ to be determined by considering D^{HF} in combination with the D-nuclear quadrupole coupling constant $\chi(D)$ for the corresponding dimer $B \cdots DF$. The assumptions are that δr is independent of the D/H isotopic substitution and that the angular oscillations β can be described by a two-dimensional, isotropic harmonic oscillator. $\chi(D)$ changes from the free DF value through the lengthening δr , the angular oscillation β' in $B \cdots DF$, and through the additional electric field gradient at D due to the presence of B. The effect of the last of these can be estimated and the experimental $\chi(D)$ corrected to give $\chi^{\text{corr}}(D)$. Then, under the constraint that the ratio β_{av}/β'_{av} is as required by the two-dimensional isotropic harmonic oscillator, it is possible to find β_{av} and δr from D^{HF} and $\chi^{\text{corr}}(D)$.

The results of carrying out the above procedure for the series $B \cdots H(D)F$, where $B = \text{Ar, Kr, Xe, N}_2, \text{CO, H}_2\text{S, HCN, CH}_3\text{CN, and H}_2\text{O}$, are set out in Figure 29, where δr (open circles) is plotted against the hydrogen-bond stretching force constant k_σ for convenience, the expectation being that δr will increase (but, of course, not necessarily linearly) as the strength of the hydrogen bond increases. This expectation is realized but we note that δr is in all cases very small, for example only 0.016 Å or 1.7% of the free HF bond length in the most strongly bound case $\text{H}_2\text{O} \cdots \text{HF}$. We conclude therefore that for these dimers $B \cdots HF$ the extent of proton transfer is negligible.

(ii) *A Simple Electrostatic Model for δr .* As mentioned in Section 4A(v) the HF molecule can be represented in useful approximation as a simple extended electric dipole with charges $q_H = 0.54 e$ and $q_F = -0.54 e$ on the H and F atoms, respectively. We imagine this dipole brought up to B along the z-axis to achieve

the observed distance $r(\text{B} \cdots \text{F})$ but with the H and F nuclei clamped at their separation in free HF. Following the Buckingham–Fowler model,⁵¹ the repulsive interaction of B and HF is represented by hard van der Waals spheres located on the acceptor atom of B and on F. The hydrogen atom is assumed to experience no repulsive interaction with B and therefore can penetrate the sphere located on B. When the HF distance is allowed to change, the hydrogen atom moves towards B under the attractive force $q_{\text{H}}dV_{\text{H}}/dz$, where dV_{H}/dz is the potential gradient at H due to B and can be calculated from the published⁵¹ DMA's of the various acceptor molecules B. The movement of H will continue until the restoring force $k_s\delta r$ due to extension δr of the HF bond just balances the electrostatic attractive force: *i.e.* until

$$q_{\text{H}}dV_{\text{H}}/dz = k_s\delta r \quad (11)$$

A route to δr is thereby provided.⁷³ Values of δr so calculated are shown as filled circles in Figure 29 for the series $\text{B} \cdots \text{HF}$. The agreement with experiment is satisfactory for such a simple electrostatic model.

(iii) *The Nature of Dimers in Ammonium Chloride Vapour: Hydrogen Bonded $\text{H}_3\text{N} \cdots \text{HCl}$ or Ion Pair $\text{H}_3\text{NH} \cdots \text{Cl}$?* We have demonstrated in (i) and (ii) above that, for a series of dimers $\text{B} \cdots \text{HF}$ at least, the extent of proton transfer from F to B is negligible (as measured by δr). Is this always so and, if not, under what conditions might a more significant extent of proton transfer be observed? Might it be possible to identify experimentally an ion-pair dimer $\text{BH}^+ \cdots \bar{\text{X}}$ in the gas phase?

An obvious way to answer these questions is to (a) increase the proton affinity of B and (b) decrease the resistance of the HX molecule to extension. The most strongly bound dimer $\text{B} \cdots \text{HF}$ appearing in Figure 29 is $\text{H}_2\text{O} \cdots \text{HF}$. Both conditions (a) and (b) are satisfied by moving to $\text{H}_3\text{N} \cdots \text{HCl}$ (the hydrogen-bond form is written now without prejudice to the eventual experimental result). Ammonium chloride is familiar as the white smoke seen in laboratories when reagent bottles of aqueous ammonia and aqueous hydrogen chloride solutions are adjacent to each other and their vapours mix. The smoke is not, of course, the vapour phase of ammonium chloride but is composed of particles of the ionic solid which is an essentially infinite array of NH_4^+ and Cl^- ions. This poses the question: what is the nature of any dimer that is formed initially when NH_3 and HCl gases mix? A celebrated early *ab initio* investigation⁷⁴ addressed this question. The possibilities are shown in Figure 30 and range from the simple hydrogen-bonded species with negligible extension of the HCl bond to the ion pair, *via* the species in which there is partial proton transfer.

We have made^{75,76} a detailed study of the rotational spectra of several

⁷³ A. C. Legon and D. J. Millen, *J. Mol. Struct.*, 1989, **193**, 303.

⁷⁴ E. Clementi, *J. Chem. Phys.*, 1967, **46**, 3851.

⁷⁵ E. J. Goodwin, N. W. Howard, and A. C. Legon, *Chem. Phys. Lett.*, 1986, **131**, 319.

⁷⁶ N. W. Howard and A. C. Legon, *J. Chem. Phys.*, 1988, **88**, 4694.

The Properties of Hydrogen-bonded Dimers from Rotational Spectroscopy

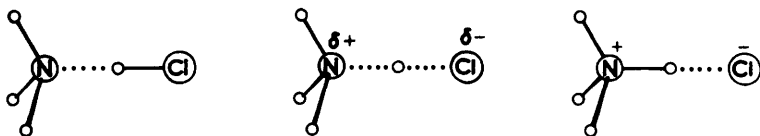


Figure 30 Three possible models of the dimer formed by NH_3 with HCl the extreme possibilities correspond to a simple hydrogen bonded species with negligible extension of the HCl bond and an ion pair in which the HCl proton has been transferred to NH_3

Table 3 Observed spectroscopic constants^a for the vibrational ground state of seven isotopomers of the dimer $\text{H}_3\text{N} \cdots \text{HCl}$

Isotopomers	B_0/MHz	D_J/kHz	D_{JK}/kHz	$\chi(\text{Cl})/\text{MHz}$
$\text{H}_3^{14}\text{N} \cdots \text{H}^{35}\text{Cl}$	4243 2593(16)	12 8(2)	371 5(8)	-47 607(9)
$\text{H}_3^{14}\text{N} \cdots \text{H}^{37}\text{Cl}$	4168 8107(9)	12 0(1)	357 7(6)	-37 531(6)
$\text{H}_3^{15}\text{N} \cdots \text{H}^{35}\text{Cl}$	4098 3113(12)	11 6(2)	344 2(5)	-47 614(5)
$\text{H}_3^{15}\text{N} \cdots \text{H}^{37}\text{Cl}$	4023 7168(10)	11 3(1)	331 4(4)	-37 527(5)
$\text{H}_3^{14}\text{N} \cdots \text{D}^{35}\text{Cl}$	4228 932(1)	12 6 ^b	—	-48 630(16)
$\text{H}_2\text{D}^{14}\text{N} \cdots \text{H}^{35}\text{Cl}$	4033 8388(16)	11 4(2)	—	-47 481(9)

^a Ref 76 ^b Calculated from k_σ of $\text{H}_3^{14}\text{N} \cdots \text{H}^{35}\text{Cl}$ and equation 2

isotopomers of $\text{H}_3\text{N} \cdots \text{HCl}$ with the aim of distinguishing between the possibilities shown in Figure 30 The pulsed-nozzle, FT microwave technique was used, with the vapour above the heated solid swept through the nozzle in a pulse of argon The spectroscopic constants determined are shown in Table 3

The symmetric-top nature of the observed spectra of species such as $\text{H}_3^{14}\text{N} \cdots \text{H}^{35}\text{Cl}$ establishes the molecular symmetry and the changes in the rotational constants B_0 with isotopic substitution establish^{75 76} beyond doubt that the order of the nuclei is $\text{H}_3\text{N} \cdots \text{H} \cdots \text{Cl}$ As expected, the hydrogen bond proton cannot be located by H/D substitution and *all* models in Figure 30 are consistent with the observed B_0 values However, two other spectroscopic constants in Table 3, the Cl-nuclear quadrupole coupling constant $\chi(\text{Cl})$ and the centrifugal distortion constant D_J , do allow us to discriminate between the models

How nuclear quadrupole coupling can be used in this respect will be illustrated by first referring to the coupling constant $\chi_0(\text{Cl})$ in free H^{35}Cl Only a limited number of discrete orientations of the angular momentum vectors I and J associated with the Cl-nuclear spin and the molecular rotation, respectively, are allowed (see Figure 31) Each allowed orientation corresponds, however, to a slightly different potential energy of interaction between the electric quadrupole moment possessed by the Cl-nucleus and the electric field gradient $V_{zz}^{(0)}$ at Cl along the molecular axis z This leads to a splitting of rotational energy levels (and therefore transitions), the extent of which is measured by $\chi_0(\text{Cl})$ It turns out that $\chi_0(\text{Cl})$ is directly related to $V_{zz}^{(0)}$ through

$$\chi_0(\text{Cl}) = -(eQ/h)\langle V_{zz}^{(0)} \rangle \quad (12)$$

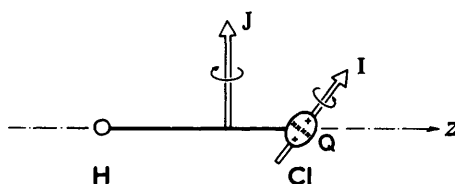


Figure 31 Mechanism of coupling of the Cl-nuclear spin angular momentum I to the framework rotational angular momentum J in the HCl molecule. The nuclear electric quadrupole moment Q interacts with the electric field gradient along the z -axis

Table 4 Comparison of ^{35}Cl -nuclear quadrupole coupling constants $\chi(^{35}\text{Cl})$ and intermolecular stretching force constants k_σ for some Cl-containing hydrogen-bonded and ionic molecules

Molecule	$\chi(^{35}\text{Cl})/\text{MHz}$	$k_\sigma/\text{N m}^{-1}$
HCl	-67.6189^a	—
$\text{HC}^{15}\text{N} \cdots \text{HCl}$	$-53.720(2)^b$	9.12^c
$\text{H}_3^{15}\text{N} \cdots \text{HCl}$	$-47.614(5)^d$	$18.2(2)^d$
$\text{Na}^+ \text{Cl}^-$	$-5.643(4)^e$	108.6^f

^a Ref. 77. ^b Ref. 79. ^c Ref. 70. ^d Ref. 76. ^e Ref. 78. ^f Ref. 83.

where e is the charge on a proton and Q is the conventional ^{35}Cl nuclear electric quadrupole moment. Hence, $\chi_0(^{35}\text{Cl}) = -67.62 \text{ MHz}^{77}$ is a measure of the electric field gradient at the Cl-nucleus.

We now consider the hydrogen-bond limiting model $\text{H}_3\text{N} \cdots \text{HCl}$ of the dimer produced when H_3N is brought up to its equilibrium position along the z -axis of HCl. As a result of the electric charge distribution of the NH_3 molecule, the electric field gradient at the Cl nucleus will change in a manner to be discussed quantitatively below. Qualitatively, however, we can note here that the change is relatively small and we expect V_{zz} , and hence $\chi(\text{Cl})$, for this model to be similar to that of free HCl. On the other hand, a more dramatic change is expected in the ion-pair model $\text{H}_3\text{NH}^+ \cdots \text{Cl}^-$. For the free Cl^- ion, the spherical symmetry of the electric charge distribution requires $V_{zz} = 0$ and hence $\chi(\text{Cl}) = 0$. The presence of the NH_4^+ ion will distort the spherical symmetry somewhat and lead to a $\chi(\text{Cl})$ of small magnitude. Such an effect is apparent in the vapour-phase ion pair $\text{Na}^+ \text{Cl}^-$, for which $\chi(\text{Cl}) = -5.6 \text{ MHz}^{78}$.

A comparison of $\chi(^{35}\text{Cl})$ values for free HCl,⁷⁷ the simple hydrogen-bonded dimer $\text{HCN} \cdots \text{HCl}$,⁷⁹ the dimer $\text{H}_3\text{N} \cdots \text{HCl}$,⁷⁶ and the ion pair $\text{Na}^+ \text{Cl}^-$ ⁷⁸ is made in Table 4. Qualitatively, the conclusion is that $\text{H}_3\text{N} \cdots \text{HCl}$ behaves like $\text{HCN} \cdots \text{HCl}$, both having $\chi(\text{Cl})$ values similar in magnitude and slightly reduced from that of free HCl. The ion pair $\text{Na}^+ \text{Cl}^-$, by contrast, has $\chi(\text{Cl})$ smaller by an order of magnitude. Also included in Table 4 are the intermolecular

⁷⁷ E. W. Kaiser, *J. Chem. Phys.*, 1970, **53**, 1686.

⁷⁸ F. H. de Leeuw, R. van Wachem, and A. Dymanus, *Symposium on Molecular Structure and Spectroscopy, Ohio*, 1969, Abstract R5.

⁷⁹ A. C. Legon, E. J. Campbell, and W. H. Flygare, *J. Chem. Phys.*, 1982, **76**, 2267.

stretching force constants k_σ calculated from centrifugal distortion constants D_J according to equation 2. Again, $\text{H}_3\text{N}\cdots\text{HCl}$ has a value closer to that of the typical hydrogen-bonded dimer $\text{HCN}\cdots\text{HCl}$ than to that of the ion pair Na^+Cl^- .

The conclusion that $\text{H}_3\text{N}\cdots\text{HCl}$ lies near to the simple hydrogen-bonded limit can be put on a quantitative basis. In the *equilibrium* conformation of the C_{3v} dimer, the Cl-nuclear quadrupole coupling constant is given by

$$\chi_{zz}(\text{Cl}) = -(eQ/h)(V_{zz}^{(0)} + \Delta V_{zz}) \quad (13)$$

where ΔV_{zz} is the shift in the electric field gradient at Cl arising from the presence of NH_3 . ΔV_{zz} is related to the external field F_z , field gradient F_{zz} , etc. evaluated at the Cl nucleus by the series expansion

$$\begin{aligned} \Delta V_{zz} = & g_{zzz} F_z + (1 + \frac{3}{2}g_{zzzz})F_{zz} + \frac{5}{2}g_{zzzzz}F_{zzz} + \frac{35}{8}g_{zzzzzz}F_{zzzz} \\ & + \quad + \frac{1}{2}e_{zzzz}F_z^2 + \quad (14) \end{aligned}$$

in which the g coefficients describe the linear response of the HCl electronic distribution to the external field, etc. For example, g_{zzz} is the electric field gradient along z induced at Cl in response to a unit external electric field. Values of coefficients shown explicitly in equation 14 have been determined *ab initio* by Baker *et al*.²¹ The field F_z and its derivatives required in equation 14 have been obtained by using Stone's distributed point multipole analysis^{51, 53} of the *ab initio* charge density of NH_3 . The value of $\chi_{zz}({}^{35}\text{Cl}) \approx -55$ MHz for the hydrogen-bonded model $\text{H}_3\text{N}\cdots\text{HCl}$ in its *equilibrium conformation* is obtained in this way. The experimental value $\chi({}^{35}\text{Cl}) = -47.6$ MHz refers to the zero-point state and will be somewhat reduced in magnitude from $\chi_{zz}({}^{35}\text{Cl})$ as a result of an angular oscillation β of HCl of the type shown for HF of $\text{HCN}\cdots\text{HF}$ in Figure 3. The agreement with experiment is therefore satisfactory and demonstrates that the description $\text{H}_3\text{N}\cdots\text{HCl}$ is appropriate. It is not necessary to invoke a significant extent of proton transfer in this case. An earlier empirical approach²⁰ that used experimental $\chi(\text{Cl})$ in a series of dimers $\text{B}\cdots\text{HCl}$ and equation 14, truncated after the first two terms, can also be applied to $\text{H}_3\text{N}\cdots\text{HCl}$. The conclusion is similarly that $\chi(\text{Cl})$ for this dimer is consistent with the value extrapolated from the more weakly bound $\text{B}\cdots\text{HCl}$ in which the extent of proton transfer is expected to be negligible.

(iv) *How Might Formation of Ion Pairs be Encouraged in the Vapour Phase? The Series $(\text{CH}_3)_{3-n}\text{H}_n\text{N}\cdots\text{HX}$* . If the extent of proton transfer is small even in $\text{H}_3\text{N}\cdots\text{HCl}$, is it possible to observe under any circumstances in the vapour phase ion pairs of the type BH^+X^- with complete proton transfer? The chemist's answer to such a question would be to increase the proton affinity of B by progressive methylation of NH_3 and/or to weaken the HX bond progressively, that is to examine either the horizontal series $(\text{CH}_3)_{3-n}\text{H}_n\text{N}\cdots\text{HCl}$, say, or the vertical series $(\text{CH}_3)_3\text{N}\cdots\text{HX}$ ($\text{X} = \text{F}, \text{Cl}, \text{Br}$) displayed in Figure 32.

We consider first the horizontal series. The ground-state rotational spectra of

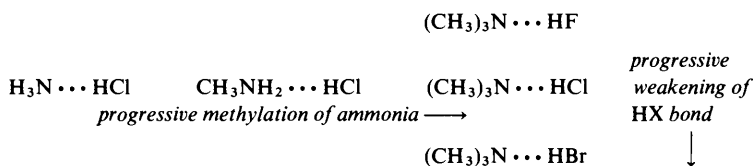


Figure 32 Series used to demonstrate the variation of the extent of proton transfer in dimers $(\text{CH}_3)_{3-n}\text{H}_n\text{N} \cdots \text{HCl}$. The horizontal series was used to show the effect of progressive methylation of NH_3 in $\text{H}_3\text{N} \cdots \text{HCl}$ and the vertical series was used to show the effect of progressively weakening the HX bond

Table 5 Comparison of ^{35}Cl -nuclear quadrupole coupling constants $\chi(^{35}\text{Cl})$ and intermolecular stretching force constants k_σ for some dimers $(\text{CH}_3)_{3-n}\text{H}_n\text{Y} \cdots \text{HCl}$, where Y = N or P

Molecule	$\chi(^{35}\text{Cl})/\text{MHz}$	$k_\sigma/\text{N m}^{-1}$
HCl	-67.6189 ^a	—
$\text{HC}^{15}\text{N} \cdots \text{HCl}$	-53.720(2) ^b	9.12 ^c
$\text{H}_3^{15}\text{N} \cdots \text{HCl}$	-47.614(5) ^d	18.2(2) ^d
$\text{CH}_3^{15}\text{NH}_2 \cdots \text{HCl}$	-37.89(1) ^e	—
$(\text{CH}_3)_3^{15}\text{N} \cdots \text{HCl}$	-21.597(3) ^f	84(3) ^f
$\text{H}_3\text{P} \cdots \text{HCl}$	-53.861(3) ^g	5.9 ^c
$(\text{CH}_3)_3\text{P} \cdots \text{HCl}$	-50.486(7) ^h	10.42(4) ^h
Na^+Cl^-	-5.643(4) ⁱ	108.6 ^j

^a Ref. 77. ^b Ref. 79. ^c Ref. 70. ^d Ref. 76. ^e Value of $\chi_{zz}(^{35}\text{Cl})$ where z is the HCl axis direction in the experimental geometry of this nonaxially symmetric dimer. See Ref. 82 for discussion. ^f Ref. 81. ^g Ref. 95. ^h Ref. 96. ⁱ Ref. 78. ^j Ref. 83.

$\text{CH}_3\text{NH}_2 \cdots \text{HCl}$ and $(\text{CH}_3)_3\text{N} \cdots \text{HCl}$ have both been detected by pulsed-nozzle, FT microwave spectroscopy and analysed to give spectroscopic constants.^{80–82} As for $\text{H}_3\text{N} \cdots \text{HCl}$, the properties most revealing of the nature of the vapour-phase dimers are $\chi(^{35}\text{Cl})$ and k_σ and these are given in Table 5 for the horizontal series shown in Figure 32. Also included for comparison are the corresponding quantities (where appropriate) for the limiting cases of the free HCl molecule and the ion pair Na^+Cl^- and for the 'typical' hydrogen-bonded dimer $\text{HCN} \cdots \text{HCl}$.

Qualitatively, we note that $\chi(^{35}\text{Cl})$ decreases smoothly in magnitude as NH_3 is progressively methylated and when methylation is complete $\chi(^{35}\text{Cl})$ is closer to the value expected in the ion-pair limit than the hydrogen-bonded limit. Quantitatively, the equilibrium value $\chi_{zz}(^{35}\text{Cl}) \approx -48$ MHz can be estimated for the *hydrogen-bonded model* of $(\text{CH}_3)_3\text{N} \cdots \text{HCl}$ by using the method outlined in (iii) above and the F_z , F_{zz} , F_{zzz} , etc. at the position eventually to be occupied by the Cl nucleus calculated with the aid of the DMA of the $(\text{CH}_3)_3\text{N}$ electric charge distribution.²³ Thus, unlike the case with $\text{H}_3\text{N} \cdots \text{HCl}$, the hydrogen bond description is inadequate to explain the observed magnitude of $\chi(^{35}\text{Cl}) = -21.6$

⁸⁰ A. C. Legon and C. A. Rego, *J. Chem. Soc., Chem. Commun.*, 1988, 1496.

⁸¹ A. C. Legon and C. A. Rego, *J. Chem. Phys.*, 1989, **90**, 6867.

⁸² A. C. Legon and C. A. Rego, *Chem. Phys. Lett.*, 1989, **162**, 369.

MHz and consequently it is necessary to invoke a substantial extent of proton transfer to describe $(\text{CH}_3)_3\text{N} \cdots \text{HCl}$ in the vapour phase.

A similar conclusion about $(\text{CH}_3)_3\text{N} \cdots \text{HCl}$ follows by considering the value $k_\sigma = 84(3) \text{ N m}^{-1}$ determined from the centrifugal distortion constant D_J .⁸¹ Qualitatively, it is not far from that (109 N m^{-1}) ⁸³ of the ion pair $\text{Na}^+ \text{Cl}^-$ which is in turn greater by an order of magnitude than the typical hydrogen-bonded value of $k_\sigma = 9.1 \text{ N m}^{-1}$ for $\text{HCN} \cdots \text{HCl}$.⁷⁰ Quantitatively, k_σ can be predicted for the *hydrogen-bond limiting model* of $(\text{CH}_3)_3\text{N} \cdots \text{HCl}$ by means of the simple empirical equation 7. It has been discussed in Section 4B how k_σ for a large number of hydrogen-bonded dimers $\text{B} \cdots \text{HX}$ can be reproduced with the aid of this relation. The values of E and N given in Table 2 have been established by using k_σ from a set of dimers known to be of the simple hydrogen-bonded type. In particular, the quantity N assigned to $(\text{CH}_3)_3\text{N}$ is the mean of the two values deduced with the aid of equation 7 from k_σ of $(\text{CH}_3)_3\text{N} \cdots \text{HF}$ ⁸⁴ and $(\text{CH}_3)_3\text{N} \cdots \text{HCN}$,⁸⁵ both of which are of the simple hydrogen-bonded type. Thus, $E = 5.0$ for HCl and $N = 14.8$ for $(\text{CH}_3)_3\text{N}$ lead to the prediction of $k_\sigma = 18.5 \text{ N m}^{-1}$ for the hydrogen-bonded limiting model $(\text{CH}_3)_3\text{N} \cdots \text{HCl}$. Clearly, this is more than a factor of four smaller than k_σ of the observed dimer.

The conclusion for the horizontal series in Figure 32 is therefore that progressive methylation of $\text{H}_3\text{N} \cdots \text{HCl}$ leads to an increasing extent of proton transfer, which becomes substantial for $(\text{CH}_3)_3\text{N} \cdots \text{HCl}$. We now consider the vertical series in Figure 32. An analysis of the type described in (iii) above applied to the HF spin-spin coupling constant D^{HF} for the symmetric top molecule $(\text{CH}_3)_3\text{N} \cdots \text{HF}$ leads to a lengthening δr of the HF bond of only $0.041(11) \text{ \AA}$ when HF takes up its equilibrium position in the dimer.⁸⁴ Thus, even for a species as strongly bound as $(\text{CH}_3)_3\text{N} \cdots \text{HF}$ (for which $k_\sigma = 39(2) \text{ N m}^{-1}$), the HF molecule is so resistant to stretching ($k_c = 966 \text{ N m}^{-1}$) that an extension of only 5% of its length occurs. That $(\text{CH}_3)_3\text{N} \cdots \text{HF}$ can be described as hydrogen-bonded is evident when the point corresponding to $\delta r = 0.04 \text{ \AA}$ and $k_\sigma = 39 \text{ N m}^{-1}$ is plotted on the axes shown in Figure 29. The point falls readily on an extrapolation of the straight line which passes through points generated by more weakly bound species.

The second member of the vertical series in Figure 32, $(\text{CH}_3)_3\text{N} \cdots \text{HCl}$, has already been discussed above. In that case a significant extent of proton transfer was invoked. The third member, $(\text{CH}_3)_3\text{N} \cdots \text{HBr}$, has also been investigated by pulsed-nozzle, FT microwave spectroscopy,⁸⁶ as has its unmethylated precursor $\text{H}_3\text{N} \cdots \text{HBr}$.⁸⁷ Again the halogen nuclear quadrupole coupling constants $\chi(^{81}\text{Br})$ and the intermolecular stretching force constants k_σ allow, through a comparison with those of free HBr ,⁸⁸ the typical hydrogen-bonded dimer

⁸³ Calculated from $\bar{\nu}_c = (2\pi c)^{-1}(k_c/\mu)^{1/2}$ using the value of $\bar{\nu}_c$ given by P. L. Clouser and W. Gordy, *Phys. Rev. A*, 1964, **134**, A863

⁸⁴ A. C. Legon and C. A. Rego, *Chem. Phys. Lett.*, 1989, **154**, 468

⁸⁵ C. A. Rego, R. C. Batten, and A. C. Legon, *J. Chem. Phys.*, 1988, **89**, 696

⁸⁶ A. C. Legon, C. A. Rego, and A. L. Wallwork, *J. Chem. Phys.*, 1990, **92**, 6397

⁸⁷ N. W. Howard and A. C. Legon, *J. Chem. Phys.*, 1987, **86**, 6722

⁸⁸ O. B. Dabbousi, W. L. Meerts, F. H. de Leeuw, and A. Dymanus, *Chem. Phys.*, 1973, **2**, 473

Table 6 Comparison of ^{81}Br -nuclear quadrupole coupling constants $\chi(^{81}\text{Br})$ and intermolecular stretching force constants k_σ for some Br-containing dimers and ionic molecules

Molecule	$\chi(^{81}\text{Br})/\text{MHz}$	$k_\sigma/\text{N m}^{-1}$
HBr	444.6807(1) ^a	—
$\text{HC}^{15}\text{N} \cdots \text{HBr}$	356.407(7) ^b	8.1 ^c
$\text{H}_3^{15}\text{N} \cdots \text{HBr}$	301.645(9) ^d	13.1(5) ^d
$(\text{CH}_3)_3^{14}\text{N} \cdots \text{HBr}$	99.645(7) ^e	82(3) ^e
$\text{Na}^+ \text{Br}^-$	48.50791 ^f	93.7 ^g

^a Ref. 88. ^b Ref. 89. ^c Ref. 70. ^d Ref. 87. ^e Ref. 86. ^f Ref. 90. ^g Ref. 91.

$\text{HCN} \cdots \text{HBr}$,^{70,89} and the ion pair $\text{Na}^+ \text{Br}^-$,^{90,91} the natures of the dimers to be deduced. The set of $\chi(^{81}\text{Br})$ and k_σ values is given in Table 6. It is clear that, on the basis of both $\chi(^{81}\text{Br})$ and k_σ , the dimer of NH_3 and HBr in the vapour above solid ammonium bromide conforms much more closely to the hydrogen-bonded description $\text{H}_3\text{N} \cdots \text{HBr}$ than to the ion-pair description $\text{H}_3\text{NH}^+ \cdots \text{Br}^-$. Evidently, the reduction in the restoring force constant k_e and the dissociation energy D_e of the HX molecule when changing from HCl to HBr is not sufficient to change the nature of the dimer $\text{H}_3\text{N} \cdots \text{HBr}$ from the hydrogen-bonded type (*i.e.* from that of the dimer $\text{H}_3\text{N} \cdots \text{HCl}$). On the other hand, the act of fully methylating the H_3N subunit in $\text{H}_3\text{N} \cdots \text{HBr}$ changes the nature of the dimer $(\text{CH}_3)_3\text{N} \cdots \text{HBr}$. Thus, both $\chi(^{81}\text{Br})$ and k_σ for $(\text{CH}_3)_3\text{N} \cdots \text{HBr}$ are close to those of $\text{Na}^+ \text{Br}^-$, which is the ion-pair limiting model in this case. Qualitatively, at least, it is also clear that the extent of proton transfer in $(\text{CH}_3)_3\text{N} \cdots \text{HBr}$ exceeds that in $(\text{CH}_3)_3\text{N} \cdots \text{HCl}$. The conclusion is therefore that not only does the extent of proton transfer increase in the series $(\text{CH}_3)_{3-n}\text{H}_n\text{N} \cdots \text{HX}$ as n decreases from 3 to 0 while X is constant but also that the extent increases for a given n (*e.g.* $n = 0$) as X changes from F through Cl to Br.

An obvious development of the approach described above for the series $(\text{CH}_3)_{3-n}\text{H}_n\text{N} \cdots \text{HX}$ is to investigate the analogous series with N replaced by P. Although the gas-phase proton affinity of phosphine is smaller than that of ammonia by 63 kJ mol⁻¹, the methyl substituent effect is much larger⁹²⁻⁹⁴ in the phosphine series $(\text{CH}_3)_{3-n}\text{H}_nP$ than in the ammonia series $(\text{CH}_3)_{3-n}\text{H}_n\text{N}$. In fact, experimental results show that the gas-phase proton affinities of $(\text{CH}_3)_3\text{N}$ and $(\text{CH}_3)_3\text{P}$ are essentially identical. In view of these observations and the change in extent of proton transfer in $\text{H}_3\text{N} \cdots \text{HCl}$ when the NH_3 molecule is

⁸⁹ E. J. Campbell, A. C. Legon, and W. H. Flygare, *J. Chem. Phys.*, 1983, **78**, 3494.

⁹⁰ J. Cederberg, D. Nitz, A. Kolan, T. Rasmusson, K. Hoffman, and S. Tufte, *Symposium on Molecular Structure and Spectroscopy, Ohio*, 1985, Abstract MF6.

⁹¹ k_e for Na Br calculated from $\bar{\nu}_e = (2\pi c)^{-1}(k_e/\mu)^{1/2}$ and the value of $\bar{\nu}_e$ given by J. R. Rusk and W. Gordy, *Phys. Rev.*, 1962, **127**, 817.

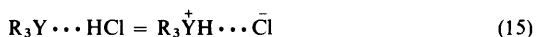
⁹² J. F. Wolf, R. H. Staley, I. Koppel, M. Taagepera, R. T. McIver, J. L. Beauchamp, and R. W. Taft, *J. Am. Chem. Soc.*, 1977, **99**, 5417.

⁹³ R. H. Staley and J. L. Beauchamp, *J. Am. Chem. Soc.*, 1974, **96**, 6252.

⁹⁴ S. Ikuta, P. Kebarle, G. M. Bancroft, T. Chan, and R. J. Puddephatt, *J. Am. Chem. Soc.*, 1982, **104**, 5899.

completely methylated, a comparison of the extent of proton transfer in $\text{H}_3\text{P}\cdots\text{HCl}$ and $(\text{CH}_3)_3\text{P}\cdots\text{HCl}$ is of particular interest. Both dimers have been examined by pulsed-nozzle, FT microwave spectroscopy.^{95,96} The chlorine nuclear quadrupole coupling constants $\chi(^{35}\text{Cl})$ and the hydrogen bond stretching force constants k_σ so obtained for these species are included in Table 5 along with those of free HCl, $\text{HCN}\cdots\text{HCl}$, $\text{H}_3\text{N}\cdots\text{HCl}$, $(\text{CH}_3)_3\text{N}\cdots\text{HCl}$, and the ion pair $\text{Na}^+\bar{\text{Cl}}$. Following the discussion set out above, the conclusion from the magnitudes of both $\chi(^{35}\text{Cl})$ and k_σ is that $\text{H}_3\text{P}\cdots\text{HCl}$ is a simple hydrogen-bonded dimer like $\text{HCN}\cdots\text{HCl}$. Although $\chi(^{35}\text{Cl})$ and k_σ change in the direction expected if an increase of ion-pair character occurs when $\text{H}_3\text{P}\cdots\text{HCl}$ is methylated to give $(\text{CH}_3)_3\text{P}\cdots\text{HCl}$, the changes are small and it is clear that the dimer $(\text{CH}_3)_3\text{P}\cdots\text{HCl}$ remains of the hydrogen-bonded rather than the ion-pair type.

The result in the preceding paragraph indicates that the proton affinity of R_3Y is not a sufficient criterion for the extent of proton transfer in $\text{R}_3\text{Y}\cdots\text{HCl}$ when $\text{Y} = \text{N}$ and P and $\text{R} = \text{H}$ or CH_3 , for otherwise we might expect the extent of proton transfer in $(\text{CH}_3)_3\text{P}\cdots\text{HCl}$ to be similar to that in $(\text{CH}_3)_3\text{N}\cdots\text{HCl}$ and this is clearly not the case. The reason why proton affinity alone is not a sufficient criterion can be seen if the contributions to the energy change for the process



are examined. It is assumed that the distance $r(\text{Y}\cdots\text{Cl})$ remains unchanged on proton transfer. Equation 15 can be written as the sum of equations 16—19



The required energy change can then be written as

$$\Delta E_{15} = \sum_{i=16}^{19} \Delta E_i \quad (20)$$

If the ΔE_i are available, ΔE_{15} is readily estimated from equation 20. Details of the assumptions necessary to obtain estimates of the individual ΔE_i have been given elsewhere⁹⁶ and the results are summarized in Table 7. The values of ΔE_{15} in the final column are in agreement with our deductions about the nature of the

⁹⁵ A C Legon and L C Willoughby, *J Chem Soc., Chem Commun.*, 1982, 997 and unpublished results

⁹⁶ A C Legon and C A Rego, *J Chem Soc., Faraday Trans.*, 1990, **86**, 1915

Table 7 Estimates of energy changes ΔE_{15} for the reaction $R_3Y \cdots HCl = R_3\overset{\dagger}{Y}H \cdots \bar{Cl}$, where $R = H$ or CH_3 and $Y = N$ or P

		$\Delta E_i/kJ\ mol^{-1}{}^a$				
Y	R	$i = 16$	17	18	19	15
N	H	42	-858	1391	-440	135
N	CH ₃	54	-945	1391	-493	7
P	H	14	-795	1391	-358	252
P	CH ₃	24	-946	1391	-385	84

^a For the origin of each of the values of ΔE_i in this table, see Ref. 96.

dimers $R_3Y \cdots HCl$ from rotational spectroscopy, for the large positive values in the cases $Y = P$, $R = H$ and CH_3 , and $Y = N$, $R = H$ indicate that the simple hydrogen-bonded form of the dimer is significantly lower in energy than the ion-pair form. On the other hand, ΔE_{15} is near to zero for $(CH_3)_3N \cdots HCl$, indicating the likelihood of a significant extent of proton transfer, as observed. The reason why the proton affinity ($-\Delta E_{17}$) alone is not a criterion of proton transfer is now evident. Although this quantity is the same for both $(CH_3)_3N$ and $(CH_3)_3P$, the presence of the counter ion \bar{Cl} leads to a greater Coulombic stabilization (ΔE_{19}) for the species $(CH_3)_3\overset{\dagger}{N}H \cdots \bar{Cl}$ than for $(CH_3)_3\overset{\dagger}{P}H \cdots \bar{Cl}$ since the distance $r(\overset{\dagger}{Y}H \cdots \bar{Cl})$ is greater in the latter case.

Finally, we note that when ΔE_{15} is similarly estimated⁸² for the series $(CH_3)_3N \cdots HX$ where $X = F$, Cl , and Br the results are roughly 200, 7, and $-25\ kJ\ mol^{-1}$, respectively. The trend in the ΔE_{15} values again follows the order of the extent of proton transfer established by rotational spectroscopy for this series.

Acknowledgements. It gives me great pleasure to acknowledge here my long scientific collaboration and personal friendship with Professor D. J. Millen. I also thank the group of research workers, low in number but high in quality, who carried out the experimental work on which this article is based. I am particularly pleased to have this opportunity to thank Debby Millard for her help in preparing this review and in many other ways. I am grateful to John Cresswell for drawing the diagrams. Much of the work described here has been supported by the Science and Engineering Research Council through research grants and studentships.